Check for updates

Research

New Phytologist

CAD1 and CCR2 protein complex formation in monolignol biosynthesis in *Populus trichocarpa*

Xiaojing Yan[1,2]*, Jie Liu[3]*, Hoon Kim[4]*, Baoguang Liu[5,6]*, Xiong Huang[1], Zhichang Yang[7], Ying-Chung Jimmy Lin[5,8], Hao Chen[3], Chenmin Yang[3], Jack P. Wang[3,5], David C. Muddiman[7], John Ralph[4], Ronald R. Sederoff[3], Quanzi Li[1,2] and Vincent L. Chiang[3,5]

[1]State Key Laboratory of Tree Genetics and Breeding, Chinese Academy of Forestry, Beijing 100091, China; [2]Research Institute of Forestry, Chinese Academy of Forestry, Beijing 100091, China; [3]Forest Biotechnology Group, Department of Forestry and Environmental Resources, North Carolina State University, Raleigh, NC 27695, USA; [4]Department of Biochemistry and DOE Great Lakes Bioenergy Research Center, Wisconsin Energy Institute, University of Wisconsin, Madison, WI 53726, USA; [5]State Key Laboratory of Tree Genetics and Breeding, Northeast Forestry University, Harbin 150040, China; [6]Department of Forestry, Beihua University, Jilin 132013, China; [7]W.M. Keck FT-ICR Mass Spectrometry Laboratory, Department of Chemistry, North Carolina State University, Raleigh, NC 27695, USA; [8]Department of Life Sciences, Institute of Plant Biology, College of Life Science, National Taiwan University, Taipei 10617, Taiwan

Authors for correspondence
Quanzi Li
Tel: +86 10 62824008
Email: liqz@caf.ac.cn

Vincent L. Chiang
Tel: +86 451 82192448
Email: vchiang@ncsu.edu

Received: *18 July 2018*
Accepted: *20 September 2018*

New Phytologist (2019) **222:** 244–260
doi: 10.1111/nph.15505

Key words: co-immunoprecipitation, enzyme activity, monolignol biosynthetic pathway, nuclear magnetic resonance (NMR), *Populus trichocarpa*, stem-differentiating xylem protein.

Summary

- Lignin is the major phenolic polymer in plant secondary cell walls and is polymerized from monomeric subunits, the monolignols. Eleven enzyme families are implicated in monolignol biosynthesis. Here, we studied the functions of members of the cinnamyl alcohol dehydrogenase (CAD) and cinnamoyl-CoA reductase (CCR) families in wood formation in *Populus trichocarpa*, including the regulatory effects of their transcripts and protein activities on monolignol biosynthesis.
- Enzyme activity assays from stem-differentiating xylem (SDX) proteins showed that RNAi suppression of *PtrCAD1* in *P. trichocarpa* transgenics caused a reduction in SDX CCR activity. RNAi suppression of *PtrCCR2*, the only CCR member highly expressed in SDX, caused a reciprocal reduction in SDX protein CAD activities. The enzyme assays of mixed and coexpressed recombinant proteins supported physical interactions between PtrCAD1 and PtrCCR2.
- Biomolecular fluorescence complementation and pull-down/co-immunoprecipitation experiments supported a hypothesis of PtrCAD1/PtrCCR2 heterodimer formation.
- These results provide evidence for the formation of PtrCAD1/PtrCCR2 protein complexes in monolignol biosynthesis *in planta*.

Introduction

Lignin is a major component of the secondary cell walls of vascular plants, accounting for >20% of the cell wall in wood (Sarkanen & Ludwig, 1971; Hu *et al.*, 1999; Higuchi, 2009). Lignin interacts with the other two major cell wall components, cellulose and hemicelluloses, creating a hydrophobic surface for water transport and conferring rigidity to the cell wall (Sarkanen & Ludwig, 1971). Lignin negatively affects cellulose digestibility and is the major barrier to lignocellulose-based biomaterial and biofuel production (Li *et al.*, 2014). An understanding of lignin biosynthesis is important for insights into plant development and adaptation, but also for many applications in which lignin could be modified to improve its utility as a feedstock for materials and energy.

Lignin is a phenolic polymer of three hydroxycinnamyl alcohols: sinapyl alcohol, coniferyl alcohol and *p*-coumaryl alcohol (Freudenberg & Neish, 1968; Sarkanen & Ludwig, 1971). These alcohol precursors are termed the S, G and H monolignols, because they result in syringyl, guaiacyl and *p*-hydroxyphenyl subunits, respectively, in the polymer. In angiosperms, lignin is polymerized primarily from S and G monolignols and trace amounts of the H monolignol. The ratio of S and G units in the wood of *Populus* is *c.* 2 : 1 (Sarkanen & Ludwig, 1971; Hu *et al.*, 1999; Higuchi, 2009), whereas, in the dicot *Arabidopsis* and the monocot switchgrass, the G units are present at two to three times that of the S units (Berthet *et al.*, 2011; Shen *et al.*, 2013). In gymnosperms, lignin is polymerized from G monolignols, with a minor amount of H monolignols: H lignin subunits are more prevalent in compression wood (Timell, 1986). Other phenylpropanoid components, such as hydroxycinnamaldehydes, hydroxycinnamates and various monolignol conjugates (acetate, *p*-hydroxybenzoate, *p*-coumarate and now ferulates) are also incorporated into lignins (Ralph, 2010; Withers *et al.*, 2012; Karlen *et al.*, 2016).

*These authors contributed equally to this work.

© 2018 The Authors
New Phytologist © 2018 New Phytologist Trust

14698137, 2019, 1, Downloaded from https://nph.onlinelibrary.wiley.com/doi/10.1111/nph.15505 by CochraneChina, Wiley Online Library on [31/01/2024]. See the Terms and Conditions (https://onlinelibrary.wiley.com/terms-and-conditions) on Wiley Online Library for rules of use; OA articles are governed by the applicable Creative Commons License

Monolignols are derived from phenylalanine (Sarkanen & Ludwig, 1971). Pathway perturbations and biochemical analyses have demonstrated that 11 enzyme families are involved in monolignol biosynthesis (Dixon *et al.*, 2001; Higuchi, 2003; Vanholme *et al.*, 2013; Wang *et al.*, 2014) (Fig. 1). These families are phenylalanine ammonia-lyase (PAL), cinnamate 4-hydroxylase (C4H), *p*-coumaroyl-CoA 3-hydroxylase (C3H), *p*-coumarate CoA ligase (4CL), hydroxycinnamoyltransferase (HCT), caffeoyl shikimate esterase (CSE), caffeoyl-CoA *O*-methyltransferase (CCoAOMT), cinnamoyl-CoA reductase (CCR), coniferaldehyde 5-hydroxylase (CAld5H, first named F5H, ferulate 5-hydroxylase), caffeic acid 3-*O*-methyltransferase (COMT) and cinnamyl alcohol dehydrogenase (CAD). PAL, C4H and 4CL convert phenylalanine to *p*-coumaroyl-CoA, which is the branch-point substrate for the flavonoid pathway (Weisshaar & Jenkins, 1998; Rohde *et al.*, 2004; Dixon *et al.*, 2006; Vogt, 2010). Coniferaldehyde can be converted to sinapaldehyde by CAld5H and COMT, and the reduction of feruloyl-CoA to coniferaldehyde is mediated by CCR (Baucher *et al.*, 1996; Lapierre *et al.*, 1999; Li *et al.*, 2005; Leple *et al.*, 2007; Vanholme *et al.*, 2008). CAD, the enzyme involved in the last step of monolignol biosynthesis, reduces substrates coniferaldehyde and sinapaldehyde to their corresponding monolignols, coniferyl and sinapyl alcohols, for G and S monolignol formation.

The characterization of the enzymes of monolignol biosynthesis has facilitated the generation of transgenics with reduced lignin content and an alteration of lignin composition. In transgenics with altered lignin content or structure resulting from the downregulation of monolignol pathway genes, the accessibility of plant cell wall polysaccharides to chemical, enzymatic and microbial digestion is increased (Baucher *et al.*, 1996; Hu *et al.*, 1999; Chen & Dixon, 2007; Bouvier d'Yvoire *et al.*, 2013; Van Acker *et al.*, 2013). Strong downregulation of *CCR*, *C3H*, *HCT* or *CAD* affects plant growth (Chen & Dixon, 2007; Leple *et al.*, 2007; Li *et al.*, 2014). Salicylic acid accumulation, not lignin content reduction, is the cause of the growth defects in the *HCT*-downregulated *Arabidopsis* (Gallego-Giraldo *et al.*, 2011), because reduction in the salicylic acid level restores the normal growth of *HCT*-downregulated plants. However, in poplar, constitutive elevation of salicylic acid does not affect plant growth (Xue *et al.*, 2013). The monolignol biosynthetic pathway is generally conserved among dicot plant species (Boerjan *et al.*, 2003; Umezawa, 2010), although the route of monolignol biosynthesis through the pathway among different plants is not exactly the same (Weng & Chapple, 2010; Shen *et al.*, 2013). Although some transcription factors have been identified to be regulators of lignin biosynthesis (Zhou *et al.*, 2009; Zhao *et al.*, 2010; Zhong *et al.*, 2010; Öhman *et al.*, 2013), an understanding of the regulation of monolignol biosynthesis and the extent of its conservation across major taxa remains limited.

With the availability of the genome sequence of *Populus trichocarpa* (Tuskan *et al.*, 2006), it is now possible to use a more comprehensive systems approach to study lignin biosynthesis during wood formation (Li *et al.*, 2014). We have identified 21 enzymes that participate in monolignol biosynthesis (Shi *et al.*, 2010; Wang *et al.*, 2014) and have generated transgenic plants in which the expression of the monolignol pathway genes is perturbed. In this article, we report the characterization of *PtrCAD1* and *PtrCCR2* RNAi transgenic plants. Our data demonstrate a protein–protein interaction of PtrCAD1 and PtrCCR2, and show that the interaction may affect their activities in the plants.

Materials and Methods

Transgenics production

Fragments of *c.* 300 bp in length were amplified from *PtrCAD1* and *PtrCCR2* cDNA (Shi *et al.*, 2010), and used as sense and antisense fragments for suppression. These were inserted in *pCR2.1-GL* (Li *et al.*, 2011) at *Spe*I/*Sac*I and *Sal*I/*BamH*I sites, respectively. For stem-differentiating xylem (SDX)-specific gene suppression, the antisense:Gus linker (GL):sense fragment was cloned into *pBI121-4CL×P* (Wang *et al.*, 2014) at *BamH*I/*Sac*I, resulting in *pBI121-4CL×P-CAD1i* (i33) and *pBI121-4CL×P-CCR2i* (i26). The primers used for vector construction are shown in Supporting Information Table S1. *Populus trichocarpa* Nisqually-1 trees, used for transformation, were grown in a glasshouse on the North Carolina State University (NCSU) campus, and the stems of five to eight internodes were sterilized and used for Agrobacterium-mediated transformation, as described previously (Song *et al.*, 2006). The stems, 1 m above the ground, from 6-month-old transgenic trees were used for developing xylem and wood sample collections. The developing xylem was scrapped with a single-edge razor, frozen and stocked in liquid nitrogen. For each line, samples were collected from three propagule plants as three biological replicates.

Quantitative reverse transcription-polymerase chain reaction (qRT-PCR)

Transcript abundance in the transgenic SDX was quantified by qRT-PCR and the primers used have been described previously (Shi *et al.*, 2010; Li *et al.*, 2011).

Enzyme assays and protein quantification of SDX proteins

SDX protein extraction and enzyme assays were performed following our established protocol (Liu *et al.*, 2012). Protein quantification was conducted as described by Shuford *et al.* (2012).

Wood chemical composition

Wood composition was determined following Lu *et al.* (2013).

Nuclear magnetic resonance (NMR) sample preparation and NMR experiments

Preparation of NMR samples, NMR experiments, data reduction, two-dimensional NMR volume integration and plotting were performed exactly as described previously (Lu *et al.*, 2013).

© 2018 The Authors
New Phytologist © 2018 New Phytologist Trust

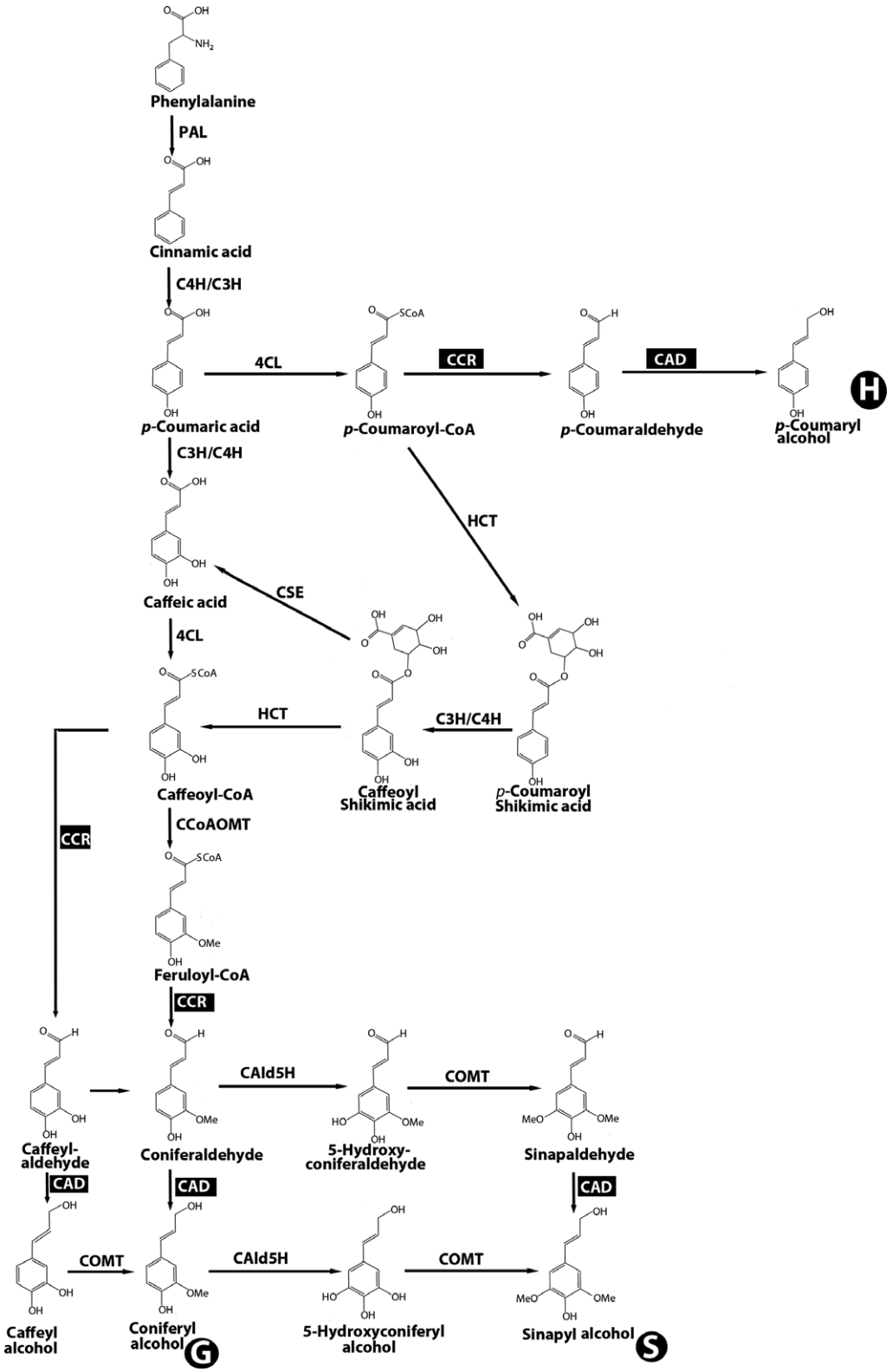

Fig. 1 Proposed monolignol pathway in *Populus* spp. Eleven enzyme families are involved in the formation of guaiacyl (coniferyl alcohol), syringyl (sinapyl alcohol) and *p*-hydroxyphenyl (*p*-coumaryl alcohol) monomers, which are called S, G and H monolignols, respectively. PAL, phenylalanine ammonia-lyase; C4H, cinnamate 4-hydroxylase; C3H, *p*-coumaroyl-CoA 3-hydroxylase; 4CL, *p*-coumarate CoA ligase; HCT, hydroxycinnamoyltransferase; CSE, caffeoyl shikimate esterase; CCoAOMT, caffeoyl-CoA *O*-methyltransferase; CCR, cinnamoyl-CoA reductase; CAld5H, coniferaldehyde 5-hydroxylase; COMT, caffeic acid 3-*O*-methyltransferase; CAD, cinnamyl alcohol dehydrogenase.

© 2018 The Authors
New Phytologist © 2018 New Phytologist Trust

14698137, 2019, 1, Downloaded from https://nph.onlinelibrary.wiley.com/doi/10.1111/nph.15505 by CochraneChina, Wiley Online Library on [31/01/2024]. See the Terms and Conditions (https://onlinelibrary.wiley.com/terms-and-conditions) on Wiley Online Library for rules of use; OA articles are governed by the applicable Creative Commons License

14698137, 2019, 1, Downloaded from https://nph.onlinelibrary.wiley.com/doi/10.1111/nph.15505 by CochraneChina, Wiley Online Library on [31/01/2024]. See the Terms and Conditions (https://onlinelibrary.wiley.com/terms-and-conditions) on Wiley Online Library for rules of use; OA articles are governed by the applicable Creative Commons License

Subcellular localization and bimolecular fluorescence complementation (BiFC) assays

The coding regions of *PtrCAD1* and *PtrCCR2* were amplified with primer sets CAD1-F/-R and CCR2-F/-R (Table S1), respectively, digested with *Xba*I/*Sal*I and cloned into *pUC19-35S-sGFP* (Chen *et al.*, 2011). The generated *pUC19-35S-CAD1:sGFP* and *pUC19-35S-CCR2:sGFP* were used for subcellular localization study.

The coding regions of *PtrCAD1* and *PtrCCR2* were PCR amplified with primer sets CAD1bi-F/-R and CCR2bi-F/-R, respectively (Table S1). The amplicons were cloned into pENTR/D-TOPO vector (Invitrogen) and sequence verified. The *PtrCAD1* and *PtrCCR2* coding sequences were then individually Gateway cloned into BiFC vectors pUGW2-nEYFP (YFP^N: amino acids 1–174) and pUGW2-cEYFP (YFP^C: amino acids 175–239) (Nakagawa *et al.*, 2007), yielding *35S-PtrCAD1:EYFP*^{N}, *35S-PtrCAD1:EYFP*^{C}, *35S-PtrCCR2:EYFP*^{N} and *35S-PtrCCR2:EYFP*^{C}. In all four BiFC constructs, the enhanced yellow fluorescent protein (EYFP) fragment was fused to the C-terminus of the gene coding sequence.

Populus trichocarpa SDX protoplast isolation and polyethylene glycol (PEG)-based transfection were carried out using the stems below the tenth internode, as described by Lin *et al.* (2014), with modifications. Briefly, debarked stem segments (10 cm each) from three glasshouse-grown 4-month-old *P. trichocarpa* plants were incubated in 40 ml of freshly prepared enzyme solution (20 mM MES (pH 5.7), 0.3 M mannitol, 20 mM KCl, 1.5% (w/v) cellulase R-10 (Yakult, Tokyo, Japan), 0.4% (w/v) Macerozyme R-10 (Yakult), 10 mM $CaCl_2$ and 0.1% (w/v) BSA) for 3 h in the dark, without shaking. The stem segments were then transferred to MMG solution (4 mM MES (pH 5.7), 0.3 M mannitol and 15 mM $MgCl_2$). After gentle swirling for 1 min, the MMG solution was filtered through a 75-μm nylon membrane. Protoplasts were collected by centrifugation of the filtrate at 300 ***g*** for 3 min, and the pellet was resuspended in 3 ml of MMG solution. The protoplast concentration was determined using a hemocytometer, and MMG solution was added to a final protoplast concentration of 2×10^5 cells ml^{-1}.

Plasmid DNA for protoplast transfection was prepared using the CsCl method (Lin *et al.*, 2014). Ten microliters of plasmid DNA (26 μg), 100 μl protoplasts (2×10^4 cells) and 110 μl of freshly prepared PEG solution (40% (w/v) PEG 4000, 0.2 M mannitol and 100 mM $CaCl_2$) were mixed in a 2-ml centrifuge tube and held at room temperature for 10 min, followed by an addition of 4.4 ml of freshly prepared Wi solution (4 mM MES (pH 5.7), 0.3 M mannitol and 20 mM KCl) to stop the transfection. Transfected protoplasts were collected by centrifugation at 500 ***g*** for 3 min and resuspended in 1 ml Wi solution; the protoplast solution was transferred into a six-bore cell culture plate (35×15 mm^2) coated with 1% (v/v) fetal bovine serum, and incubated at room temperature in the dark for 7–12 h. After transfection, YFP fusion protein fluorescence images were recorded using an LSM 700 (Zeiss) confocal laser scanning microscope.

Antibody production

The PtrCAD1-specific peptide VVGEVVEVGSDVTKF was selected for rabbit polyclonal antibody production, and the PtrCCR2-specific peptide GAVYMDPNKGPDVVID was selected for rabbit and goat polyclonal antibody production The antibodies were produced as described previously (Li *et al.*, 2012).

Pull-down assays in *Escherichia coli*

pGEXKG-PtrCAD1 and *pGEXKG-PtrCCR2* were used for glutathione *S*-transferase (GST) fusion protein expression in *E. coli* (Shuford *et al.*, 2012). For histidine (His)-tagged protein expression, *PtrCAD1* and *PtrCCR2* coding regions were amplified with primer sets CAD1Duet-F/-R and CCR2Duet-F/-R (Table S1), respectively, and cloned into pRSFDuet-1 vectors (Novagen, Madison, WI, USA) at *Sac*I/*Sal*I, generating Duet-PtrCAD1 and Duet-PtrCCR2. The pGEXKG-1-derived and RSFDuet-derived plasmids were cotransformed into *E. coli* BL21 (DE3) (Invitrogen). After induction with 0.4 mM isopropyl β-D-1-thiogalactopyranoside (IPTG) at 25°C for 12 h, cells were collected from a 50-ml culture, suspended in 10 ml of buffer (1 × PBS, 2 mM EDTA, 0.1% β-mercaptoethanol, 1 mM phenylmethylsulfonyl fluoride (PMSF), 1 μg ml^{-1} leupeptin and 1 μg ml^{-1} pepstatin) and disrupted by sonication, followed by centrifugation at 10 000 ***g*** at 4°C for 30 min. Soluble protein (500 μg) was mixed with 10 μl of rat monoclonal anti-GST antibodies (Sigma) in 500 μl of binding buffer (1 × PBS, 2 mM EDTA, 1% Nonidet P40 (NP40), 1% (w/v) BSA, 0.1% β-mercaptoethanol, 1 μg ml^{-1} leupeptin and 1 μg ml^{-1} pepstatin) and incubated for 1 h with agitation at 4°C. Dynabeads Protein G (20 μl; Invitrogen) was added, and binding was continued for 3 h. The Dynabeads were washed with 800 μl of binding buffer, in which BSA was omitted, for five times at 4°C, each time for 10 min. The beads were resuspended in 32 μl of 2 × sodium dodecylsulfate-polyacrylamide gel electrophoresis (SDS-PAGE) sample buffer and boiled for 10 min to elute the proteins. A 15-μl aliquot was loaded onto a 10% SDS-PAGE gel and western blotting was conducted with mouse monoclonal anti-His antibodies (1 : 12 000 dilution; Invitrogen) as primary antibodies, anti-mouse immunoglobulin G (IgG) horseradish peroxidase (HRP) conjugate (1 : 20 000 dilution; Promega) as secondary antibodies and SuperSignal West Pico chemiluminescent substrate (Thermo Scientific, San Jose, CA, USA) for signal detection. The immunoprecipitated products were also probed with either rabbit anti-PtrCAD1 antibodies (1 : 3000 dilution) or anti-PtrCCR2 antibodies (1 : 3000 dilution) for the detection of PtrCAD1 and PtrCCR2.

Pull-down assays in SDX

Escherichia coli-expressed PtrCCR2 GST fusion proteins (Shuford *et al.*, 2012) were purified using reduced glutathione. SDX tissue (4 g) was ground in an analytical mill (IKA, Model A11 basic, Staufen, Germany) and transferred into 20 ml of binding buffer (1 × PBS, 1% NP40, 2 mM EDTA, 5 mM dithiothreitol

© 2018 The Authors
New Phytologist © 2018 New Phytologist Trust

14698137, 2019, 1, Downloaded from https://nph.onlinelibrary.wiley.com/doi/10.1111/nph.15505 by CochraneChina, Wiley Online Library on [31/01/2024]. See the Terms and Conditions (https://onlinelibrary.wiley.com/terms-and-conditions) on Wiley Online Library for rules of use; OA articles are governed by the applicable Creative Commons License

(DTT), 20 mM sodium ascorbate, 10% (w/w) polyvinylpolypyrrolidone, 1 mM PMSF, 1 μg ml^{-1} leupeptin and 1 μg ml^{-1} pepstatin). After a brief homogenization, the mixture was centrifuged for 1 h at 16 000 ***g*** at 4°C. Each 8-ml supernatant was mixed with 400 μg PtrCCR2 GST fusion proteins and 400 μg GST proteins, respectively. The mixture was incubated at 4°C with shaking for 3 h. Glutathione-*S*-agarose beads (200 μl; Sigma) were added, and shaking was continued for 2 h at 4°C. The beads were washed with 50 ml of wash buffer (1 × PBS, pH 7.4, 5 mM EDTA, 1% Triton X-100, 0.1% β-mercaptoethanol, 1 μg ml^{-1} leupeptin and 1 μg ml^{-1} pepstatin) and resuspended in 200 μl of 2 × protein loading buffer (20 mM Tris-HCl, pH 8.0, 100 mM DTT, 2% (w/v) SDS, 20% glycerol and 0.016% bromophenol blue). A 20-μl aliquot was boiled, spun down and used for western blotting with anti-PtrCAD1 polyclonal antibodies (1 : 5000 dilution).

Co-immunoprecipitation (Co-IP) in SDX

The immunoprecipitation experiments with goat anti-PtrCCR2 polyclonal antibodies were conducted with SDX proteins, which were extracted using the binding buffer, as described above. Dynabeads Protein G (30 μl) and 30 μl of antibodies were added to 1 ml of SDX proteins, and the mixture was incubated with rotation at 4°C for 12 h. After washing with 1 × PBS, pH 7.4, 5 mM EDTA, 1% NP40, 0.1% β-mercaptoethanol, 1 μg ml^{-1} leupeptin and 1 μg ml^{-1} pepstatin, six times, the beads were suspended in 30 μl of protein loading buffer. After boiling, western blotting was carried out with mouse anti-PtrCAD1 antibodies.

High-performance liquid chromatography (HPLC) analysis of catalytic efficiency for the PtrCAD1/PtrCCR2 interaction

Recombinant proteins of PtrCAD1 and PtrCCR2 were expressed using *E. coli* strain Rosetta™ 2 (DE3) (Novagen) and purified using glutathione-*S*-agarose beads, as described previously (Shuford *et al.*, 2012). The purified recombinant protein concentration was determined using the Bradford reagent and verified for purity using SDS-PAGE/Coomassie brilliant blue R-250 and western blot. The substrates were mixed with assay buffers to a final volume of 100 μl, as described previously (Liu *et al.*, 2012; Wang *et al.*, 2014). The mixture was held at 30°C for 1 min, followed by the addition of protein mixtures (at molar ratios specified on the *x*-axis of Fig. 9, see later) to initiate enzymatic reactions, at 30°C for 10 min. Reactions were terminated by adding 50 μl of stop buffer containing 6% (w/v) trichloroacetic acid and 50% (v/v) acetonitrile. The substrates and products of the enzyme assays were separated on an Agilent ZoRBAX SB-C18 5 μm, 4.6 mm × 150 mm column (Agilent, Santa Clara, CA, USA), using a gradient method (solvent A, 10 mM formic acid in water; solvent B, 10 mM formic acid in acetonitrile; 10–60% B in 16 min, 60–100% B in 2 min; flow rate, 1.5 ml min^{-1}). Reaction substrates and products were detected using an Agilent 1260 diode array detector and quantified based on authentic compounds. For the enzyme assays using coexpressed proteins, we used the two crude protein extracts from the enzyme assays in *E. coli*. One is coexpressed His:PtrCAD1 and GST, and the other is coexpressed His:PtrCAD1 and GST:PtrCCR2. Western blotting was conducted to ensure the same PtrCAD1 quantities in these two crude proteins. The enzyme assay conditions were the same as in the mixed enzyme assays.

Results

RNAi downregulation of *PtrCAD1* in the SDX of *P. trichocarpa*

Although the function of CAD in lignin biosynthesis has been studied extensively in many plant species (Vanholme *et al.*, 2010), knowledge is lacking on how CAD affects metabolic fluxes in the monolignol biosynthetic pathway. We conducted a broad study of the effects of CAD member suppression on monolignol pathway enzyme abundance, metabolic flux and cell wall composition. We selected *PtrCAD1*, the only CAD member that is specifically and abundantly expressed in SDX (Shi *et al.*, 2010), as a target for RNAi knockdown. A 289-bp fragment from *PtrCAD1* was used as antisense and sense fragment, and the antisense:Gus linker (GL):sense fragment, driven by a xylem-specific *4CL* promoter (Wang *et al.*, 2014), was used for xylem-specific target knockdown. The transgenic plants grown in a glasshouse did not show obvious biomass penalty and exhibited the typical red xylem phenotypes, with different levels of coloration in different lines (Fig. S1). Based on the target gene expression in SDX from ten transgenic lines, three lines with distinct levels of gene perturbation (i33-2, i33-5 and i33-10) were selected for protein quantification, cell wall composition determination, enzyme assays and lignin NMR analysis.

In the three selected lines (i33-2, i33-5 and i33-10), *PtrCAD1* transcripts were reduced by 77.3%, 91.9% and 34.0% (Fig. 2a), respectively. The PtrCAD1 protein quantities in these three lines showed a similar reduction, with the greatest reduction (94.9%) in i33-5 (Fig. 2b). Downregulation of *PtrCAD1* caused a reduction in SDX CAD activity towards both coniferaldehyde and sinapaldehyde (Fig. 2c). Compositional analysis of the *PtrCAD*1 knockdown transgenic wood showed a 7.1–9.2% reduction in lignin content (Table 1), consistent with previous *CAD* knockdown in other species, such as the *gold hull and internode2* rice mutant (Zhang *et al.*, 2006), although a higher level of reduction was observed in the transgenics or mutants of other species, including *P. tremula* × *alba* and loblolly pine (MacKay *et al.*, 1997; Halpin *et al.*, 1998; Lapierre *et al.*, 1999; Bouvier d'Yvoire *et al.*, 2013). An increase in arabinan content and a decrease in mannan content were observed (Table 1); the reasons for these changes are not obvious.

To further understand the effects of *PtrCAD1* suppression on lignin biosynthesis, we analyzed the RNAi knockdown transgenic wood for lignin structural components and the distribution of the linkages between monomeric units using NMR spectroscopy. CAD enzymes catalyze the conversion of hydroxycinnamaldehydes to their corresponding hydroxycinnamyl alcohols. In the *PtrCAD1* knockdown transgenics, the significant changes in

© 2018 The Authors
New Phytologist © 2018 New Phytologist Trust

14698137, 2019, 1, Downloaded from https://nph.onlinelibrary.wiley.com/doi/10.1111/nph.15505 by CochraneChina, Wiley Online Library on [31/01/2024]. See the Terms and Conditions (https://onlinelibrary.wiley.com/terms-and-conditions) on Wiley Online Library for rules of use; OA articles are governed by the applicable Creative Commons License

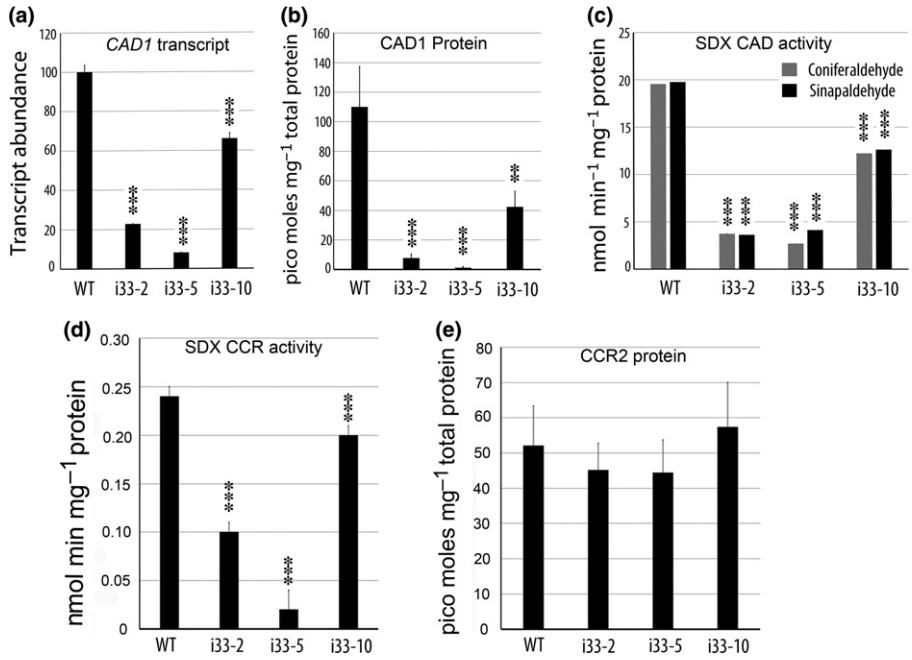

Fig. 2 Downregulation of *PtrCAD1* by RNAi in *Populus trichocarpa*. (a) *PtrCAD1* transcript abundance in the three knockdown transgenic lines (i33-2, i33-5 and i33-10) and wild-type (WT). (b) Protein quantification of PtrCAD1 in *PtrCAD1* knockdown transgenics. (c) Enzyme activities of the stem-differentiating xylem (SDX) cinnamyl alcohol dehydrogenase (CAD) family in *PtrCAD1* knockdown transgenic plants. Gray bars represent the SDX enzyme activities of conversion of coniferaldehyde to coniferyl alcohol. Black bars represent the SDX enzyme activities of conversion of sinapaldehyde to sinapyl alcohol. (d) SDX protein enzyme activities of conversion of feruloyl-CoA to coniferaldehyde. (e) PtrCCR2 protein quantification in *PtrCAD1* knockdown transgenics. Errors bars represent SE of three biological replicates. Asterisks highlight significant differences by Student's *t*-test: **, $P < 0.01$; ***, $P < 0.001$.

Table 1 Composition of *PtrCAD1* and *PtrCCR2* knockdown transgenics.

	Lignin (Klason + acid-soluble)	Arabinose	Xylose	Mannose	Galactose + rhamnose	Glucose
WT	23.48 ± 0.28	0.39 ± 0.11	17.11 ± 0.58	3.01 ± 0.22	1.37 ± 0.05	48.16 ± 1.48
i33-2	21.32 ± 0.25**	4.32 ± 0.09***	15.63 ± 0.11	1.67 ± 0.15**	1.24 ± 0.12	43.82 ± 1.26
i33-5	21.82 ± 0.40*	3.81 ± 0.51**	16.60 ± 0.54	1.60 ± 0.17**	1.33 ± 0.12	40.76 ± 2.54
i33-10	21.82 ± 0.98	3.94 ± 0.68**	14.67 ± 0.19*	1.57 ± 0.13**	1.11 ± 0.13	42.58 ± 2.28
WT	24.13 ± 0.33	0.43 ± 0.04	16.40 ± 0.42	2.22 ± 0.08	1.47 ± 0.05	46.33 ± 0.73
i26-4	16.30 ± 2.71*	2.78 ± 0.05***	15.32 ± 0.98	1.82 ± 0.02**	1.19 ± 0.04*	42.55 ± 0.15**
i26-9	21.02 ± 0.33**	3.20 ± 0.11***	13.28 ± 0.36*	1.79 ± 0.01**	1.20 ± 0.02**	42.20 ± 0.98*
i26-10	21.47 ± 0.23**	2.97 ± 0.05***	13.84 ± 0.34*	1.85 ± 0.03*	1.23 ± 0.04*	38.48 ± 1.54**

Values are means ± SE, representing three biological replicates. WT, wild-type. Values are expressed as weight percent based on vacuum-dried extract-free wood weight. Asterisks highlight significant differences by Student's *t*-test: *, $P < 0.05$; **, $P < 0.01$; ***, $P < 0.001$.

lignin were the increased aldehyde components, which can be most readily seen in the aldehyde regions ($^{13}C/^{1}H$; 183–197 ppm/9.0–10.5 ppm) of the two-dimensional heteronuclear single-quantum coherence (HSQC) NMR spectra (see later, Fig. 4). The aldehyde compositions were estimated from the aromatic regions of the spectra (Fig. 3). Transgenic line i33-10 had 10.3% aldehydes, similar to the level of the wild-type (9.7%). Line i33-5 had the highest level of aldehyde components at 29.2-%. An increased aldehyde component was also observed in i33-2, which had 14.9% aldehydes. These results indicate the successful downregulation of *PtrCAD1* and inhibition of the aldehyde-to-alcohol conversion. Normal S, G and H units exhibited altered distributions (less total %S) relative to the wild-type (Fig. 3), except in the i33-10 line, which had the lowest level of transcript reduction and, consequently, also the lowest level of new hydroxycinnamaldehyde cross-coupling products (as described below).

The aromatic region in all three *PtrCAD1* transgenic lines showed the appearance of new cross-coupled 8-*O*-4 hydroxycinnamaldehyde structures (Fig. 4), indicating how the accumulated aldehydes were incorporated into the lignin polymer. The wild-type lignin's aldehydes were primarily endgroup benzaldehydes (SA and V) and cinnamaldehydes (X), which result from the coupling of monolignols (at their β-positions) with the monomers syringaldehyde, vanillin, sinapaldehyde and coniferaldehyde. Their levels were not significantly changed in the CAD-downregulated transgenics. Importantly, the substantially enhanced peaks in Fig. 4(b, c), especially, were from

© 2018 The Authors
New Phytologist © 2018 New Phytologist Trust

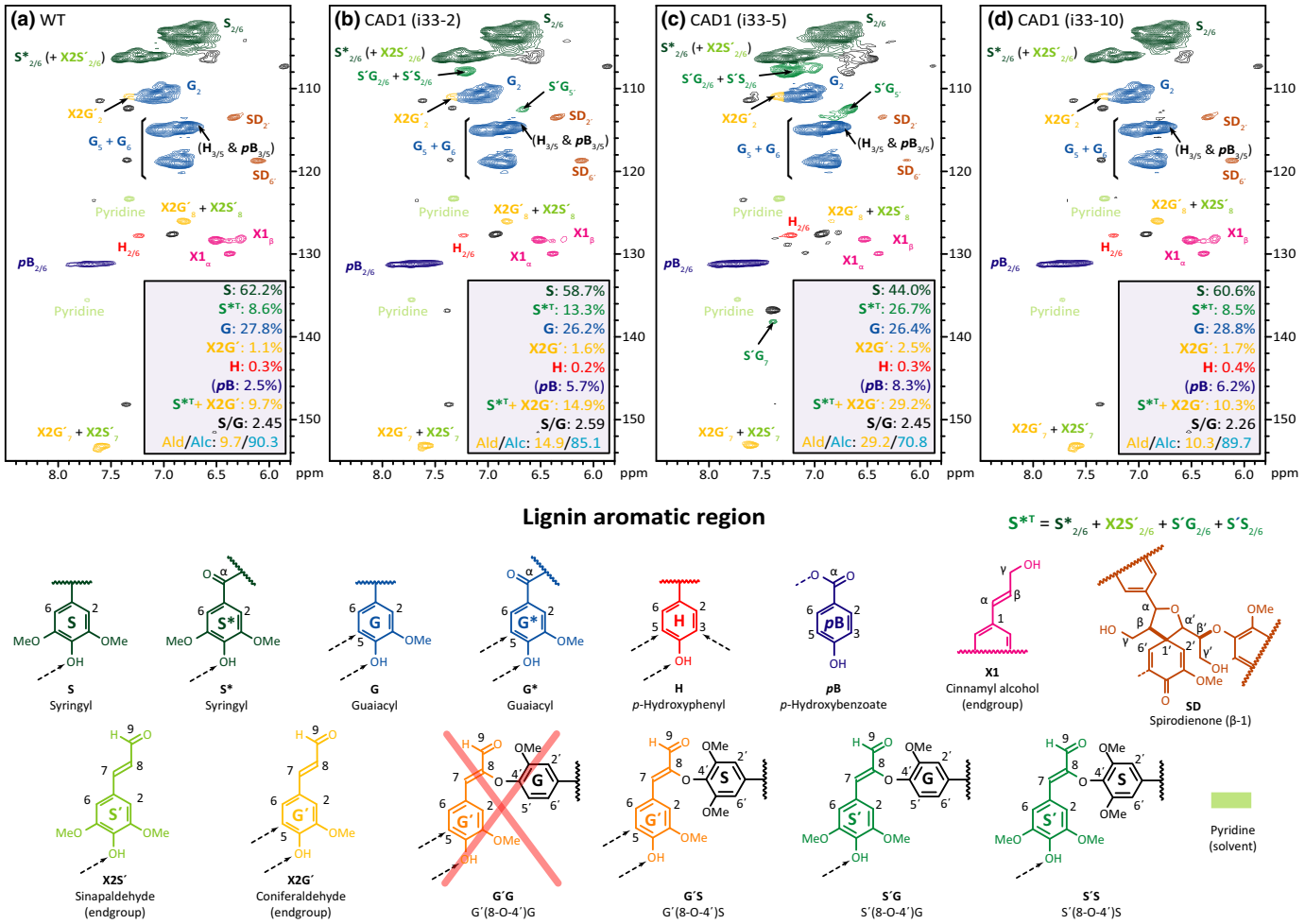

Fig. 3 Two-dimensional heteronuclear single-quantum coherence (HSQC) nuclear magnetic resonance (NMR) spectra of cellulolytic enzyme lignins (CELs) from *Populus trichocarpa CAD1* (*PtrCAD1*) knockdown transgenic wood shows the lignin aromatic region of (a) wild-type (WT), (b) i33-2, (c) i33-5 and (d) i33-10. The quantification values shown are for relative comparisons of the lignin components determined from NMR contour volume integrals. Aromatic structures of aldehydes (Ald) were compared with the traditional lignin aromatics (Alc). All correlations from the $S_{2/6}$, $S^*_{2/6}$, G_2, $X2G'_2$ and $H_{2/6}$ units sum to 100%. The S-unit aldehyde (S^{*T}) amounts were estimated ($S^*_{2/6} + X2S'_{2/6} + S'G_{2/6} + S'S_{2/6}$) first, and the coniferaldehyde endgroups ($X2G'_2$) added; the total aldehydes were estimated as $S^{*T} + X2G'$. *p*B is a lignin appendage derived from lignification using monolignol *p*-hydroxybenzoates and is not considered to be a lignin unit *per se*. Correlation peaks are colored to match those of the structures below.

hydroxycinnamaldehydes which had cross-coupled, at their 8-positions, with the phenolic end of the growing polymer – S′G from the cross-coupling of sinapaldehyde with guaiacyl (G) phenolic end-units in the polymer, and G′S and S′S by the analogous cross-coupling of coniferaldehyde or sinapaldehyde with syringyl (S) phenolic end-units. Clearly, this occurs, as has been noted previously (Kim *et al.*, 2000, 2003), when the hydroxycinnamaldehyde monomers are delivered to the wall at a sufficient level and rate that they cross-couple into the polymer, and are not simply the products of coupling reactions with the major monolignols as in the wild-type plants. There are three different combinations of aldehyde cross-coupling structures, G′S, S′G and S′S, observed in transgenic plants (Fig. 4). The G′G combination could not be detected in the transgenics, consistent with previous studies which showed that coniferaldehyde cannot 8-O-4 couple with guaiacyl units (Kim *et al.*, 2000, 2003). Aldehyde 8-8 structures also appeared in the *CAD1* transgenic, as might be expected, as a result of the delivery of enhanced levels of the hydroxycinnamaldehydes to the cell wall, allowing modest levels of dimerization to start a lignin polymer chain.

RNAi suppression of *PtrCAD1* results in a reduction in the SDX CCR enzyme activity

To investigate how suppression of *PtrCAD1* affects the metabolic flux in the monolignol pathway, we determined the SDX activities of other monolignol biosynthetic pathway enzyme families in the three *PtrCAD1* downregulated transgenics and the wild-type using our developed protocols (Liu *et al.*, 2012). Seven enzyme families were examined for SDX enzyme activity, and the enzyme activities of some families were affected (Table S2). We performed Pearson correlation and linear regression analysis to examine whether the activity reduction is correlated with PtrCAD1 activity in *PtrCAD1*/*PtrCCR2* RNAi transgenics

© 2018 The Authors
New Phytologist © 2018 New Phytologist Trust

14698137, 2019, 1, Downloaded from https://nph.onlinelibrary.wiley.com/doi/10.1111/nph.15505 by CochraneChina, Wiley Online Library on [31/01/2024]. See the Terms and Conditions (https://onlinelibrary.wiley.com/terms-and-conditions) on Wiley Online Library for rules of use; OA articles are governed by the applicable Creative Commons License

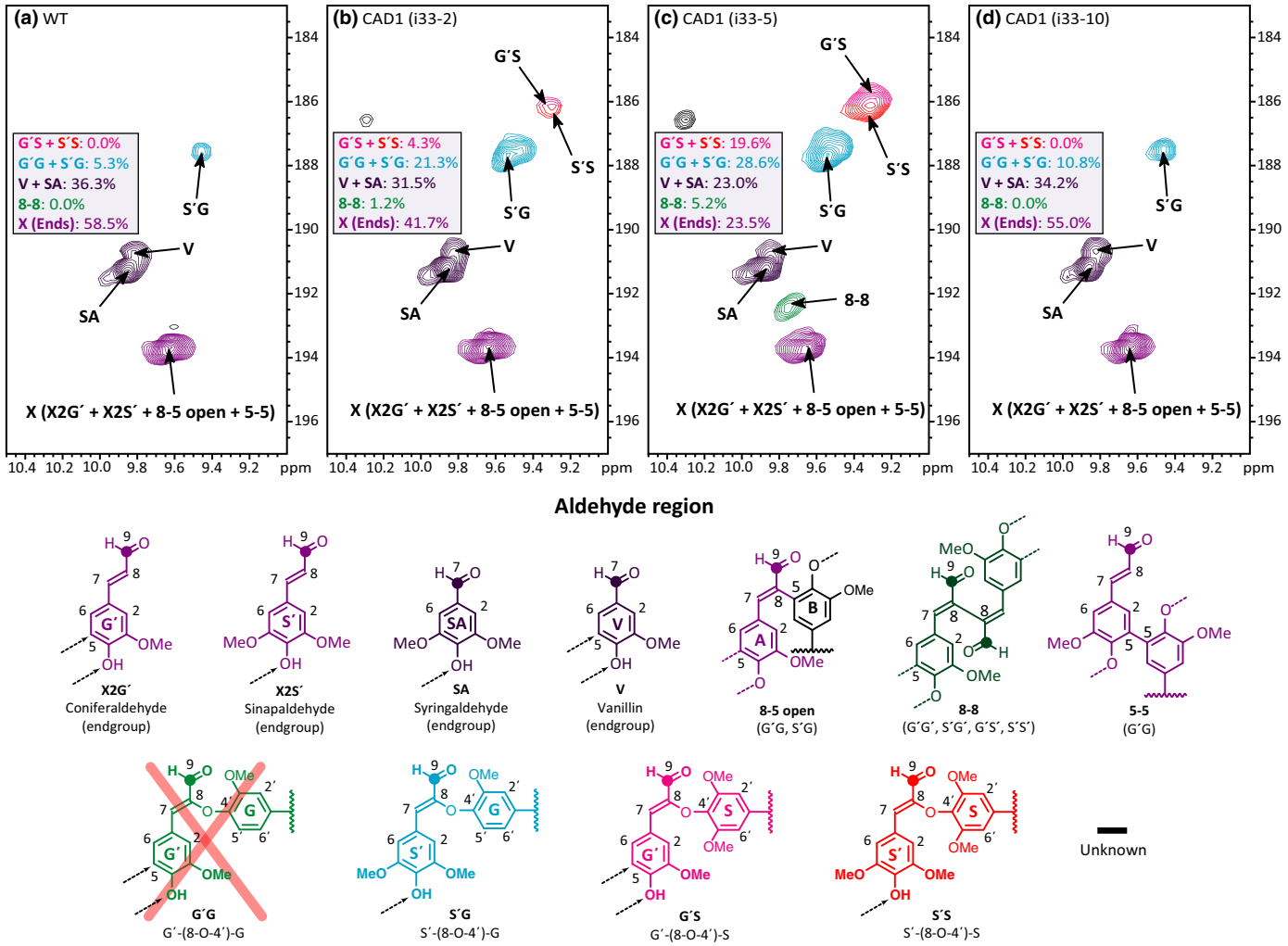

Fig. 4 Heteronuclear single-quantum coherence (HSQC) nuclear magnetic resonance (NMR) spectra of cellulolytic enzyme lignins (CELs) from *Populus trichocarpa CAD1* (*PtrCAD1*) knockdown transgenic wood shows the various aldehyde structures in (a) wild-type (WT), (b) i33-2, (c) i33-5 and (d) i33-10. The origin of the various correlation peaks, colored here to match their structures below, is described in the Results section.

(Tables S3–S6). The enzyme activities of three families, including PAL, HCT and CCR, were correlated with CAD activities of conversion of coniferaldehyde to coniferyl alcohol (Tables S3, S4), and the enzyme activities of four families, including PAL, C4H, HCT and CCR, were correlated with CAD activities of conversion of sinapaldehyde to sinapyl alcohol (Tables S5, S6). CCR is the only family whose activities have positive correlations with CAD activities (Tables S4, S6). The CCR activity reduction was 58.3%, 91.2% and 16.7% in i33-2, i33-5 and i33-10, respectively, a reduction pattern that was consistent with that for CAD. The protein abundances of PtrCCR2 in the three transgenic lines and the wild-type were essentially the same (Fig. 2e), indicating that the reduction in SDX CCR activity was not caused by PtrCCR2 protein quantity. We propose that PtrCAD1 and PtrCCR2 may undergo physical interactions, with the reduction in CCR enzyme activity being caused by a disruption of the PtrCAD1/PtrCCR2 interaction. Next, we used BiFC and pull-down/Co-IP to test for the physical interactions between these two proteins.

PtrCAD1 and PtrCCR2 form homodimers and heterodimers *in vivo*

Both PtrCAD1 and PtrCCR2 revealed their cytoplasmic location in the *P. trichocarpa* SDX protoplasts (Fig. 5a,b). For BiFC assays, we generated four constructs for the expression of PtrCAD1 and PtrCCR2 fused to the N-terminal fragment of EYFP ($EYFP^N$) or the C-terminal fragment of EYFP ($EYFP^C$), respectively. When 35S-PtrCAD1:$EYFP^N$ and 35S-PtrCCR2:$EYFP^C$ were cotransfected in *P. trichocarpa* SDX protoplasts, we observed fluorescence in the cytoplasm (Fig. 5c). Reciprocally, fluorescence was observed when 35S-PtrCAD1:$EYFP^C$ and 35S-PtrCCR2:$EYFP^N$ were coexpressed (Fig. 5d). To ensure the detection of specific interactions, we used β-glucuronidase (GUS) fused to the EYFP fragment as the negative control. No fluorescence signal was observed in the protoplasts overexpressing *PtrCAD1:*$EYFP^N$ and *GUS:*$EYFP^C$ (Fig. 5e), *PtrCAD1:*$EYFP^C$ and *GUS:*$EYFP^N$ (Fig. 5f), *PtrCCR2:*$EYFP^N$ and *GUS:*$EYFP^C$ (Fig. 5g) or *PtrCCR2:*$EYFP^C$ and *GUS:*$EYFP^N$ (Fig. 5h). The

© 2018 The Authors
New Phytologist © 2018 New Phytologist Trust

14698137, 2019, 1, Downloaded from https://nph.onlinelibrary.wiley.com/doi/10.1111/nph.15505 by CochraneChina, Wiley Online Library on [31/01/2024]. See the Terms and Conditions (https://onlinelibrary.wiley.com/terms-and-conditions) on Wiley Online Library for rules of use; OA articles are governed by the applicable Creative Commons License

BiFC results support our hypothesis that PtrCAD1 and PtrCCR2 interact. In addition, cytoplasmic fluorescence signals were observed in the SDX protoplasts coexpressing PtrCAD1:EYFP^N and PtrCAD1:EYFP^C (Fig. 5i), and in the protoplasts coexpressing PtrCCR2:EYFP^N and PtrCCR2:EYFP^C (Fig. 5j), indicating that PtrCAD1 and PtrCCR2 themselves each form homodimers.

Pull-down and Co-IP assays

To provide further evidence for PtrCAD1 and PtrCCR2 interaction, we generated six types of *E. coli* cells, each with the coexpression of two proteins. GST was fused at the N-terminal of one protein, and 6 × His was fused at the N-terminal of the other protein. The two proteins are GST- and His-tagged PtrCAD1 in cell 1 (Fig. 6a, lane 1), GST-fused PtrCAD1 (GST:PtrCAD1) and His-tagged PtrCAD1 (His:PtrCAD1) in cell 2 (Fig. 6a, lane 2), GST-fused PtrCCR2 (GST:PtrCCR2) and His:PtrCAD1 in cell 3 (Fig. 6a, lane 3), GST and His:PtrCCR2 in cell 4 (Fig. 6a, lane 4), GST:PtrCCR2 and His:PtrCCR2 in cell 5 (Fig. 6a, lane 5), and GST:PtrCAD1 and His:PtrCCR2 in cell 6 (Fig. 6a, lane 6). Immunoprecipitation was conducted with *E. coli* total proteins from each of the six types of cell by monoclonal anti-GST antibodies to pull down GST fusion proteins. The immunoprecipitates were analyzed by western blotting of monoclonal anti-His antibodies to detect His-tagged proteins. When GST:PtrCCR2 and His:PtrCAD1 were coexpressed in cell 3, His:PtrCAD1 was detected in the immunoprecipitates pulled down by anti-GST antibodies (Fig. 6a-iii, lane 3). The immunoprecipitates were further probed with anti-PtrCAD1 antibodies, and the band (Fig. 6a-iv, lane 3) confirmed that GST:PtrCCR2 could pull down His:PtrCAD1. Reciprocally, the pull-down assays in cell 6 showed the signal of His:PtrCCR2 detected by anti-His antibodies (Fig. 6a-iii, lane 6) and anti-PtrCCR2 antibodies (Fig. 6a-iv, lane 6), indicating that His:PtrCCR2 was pulled down by GST:PtrCAD1. When only GST was coexpressed with His:PtrCAD1 or His:PtrCCR2, neither of these two His-tagged proteins could be pulled down by anti-GST antibodies (Fig. 6a-iii, lanes 1 and 4). The pull-down assays support the BiFC demonstration of heterodimer formation between PtrCAD1 and PtrCCR2. Similarly, the results of pull-down assays from cells coexpressing GST:PtrCAD1 and His:PtrCAD1 (Fig. 6a, lane 2), and coexpressing GST-PtrCCR2 and His:PtrCCR2 (Fig. 6a, lane 5), support the homodimer formation of PtrCAD1 and PtrCCR2.

To detect the *in vivo* interactions of PtrCAD1 and PtrCCR2, we conducted pull-down assays in SDX. SDX crude lysates were mixed with purified PtrCCR2:GST fusion proteins and glutathione-*S*-agarose beads. Glutathione-*S*-agarose beads were used to pull down PtrCCR2:GST fusion proteins. If PtrCAD1 and PtrCCR2 interact to form complexes, the beads should also pull down PtrCAD1. The mixture was purified with glutathione-*S*-agarose beads and the purified product was subjected to western blotting by anti-PtrCAD1 antibodies. The size of the detected PtrCAD1 band by pull-down (Fig. 6b-i, lane 3) was the same as that on immunoblot with SDX crude proteins (Fig. 6b-i, lane 1). When GST and glutathione-*S*-agarose beads were mixed with SDX crude lysates, PtrCAD1 was not detected on the immunoblot (Fig. 6b-i, lane 2), eliminating the possibility of nonspecific binding.

Next, Co-IP was carried out to verify the complex formation of PtrCAD1 and PtrCCR2 in SDX. We used anti-PtrCCR2 antibodies to immunoprecipitate PtrCCR2, and the precipitates were subjected to western blotting detection using anti-PtrCAD1 antibodies to determine whether PtrCAD1 can be co-immunoprecipitated. To avoid the band of the heavy chain of anti-PtrCCR2 antibodies in the immunoblot, we used anti-PtrCCR2 goat antibodies for immunoprecipitation and anti-PtrCAD1 mouse antibodies for western blotting. The Co-IP results showed that PtrCAD1 was detected in the precipitates pulled down by anti-PtrCCR2 antibodies (Fig. 6c, lane 3), with the same size as from western blotting using SDX protein as the input (Fig. 6c, lane 1). In the control using preimmune serum in Co-IP, PtrCAD1 was not detected (Fig. 6c, lane 2). Both pull-down assays and Co-IP confirm an interaction of PtrCAD1 and PtrCCR2 in SDX.

Suppression of *CCR* gene expression results in a reduction in CAD enzyme activity in SDX

BiFC and Co-IP provide strong evidence of complex formation between PtrCAD1 and PtrCCR2, and the downregulation of *PtrCAD1* caused a reduction in CCR activities in SDX (Fig. 2d; Table S2). We further tested whether suppression of the expression of *CCR* would also affect the CAD activity in SDX.

We therefore used RNAi to suppress the expression of *PtrCCR2* in transgenic *P. trichocarpa*. *PtrCCR2* is the only wood formation-related *CCR* member expressed in *P. trichocarpa* SDX (Shi *et al.*, 2010). Ten transgenic lines were generated and three lines, i26-4, i26-9 and i26-10, with 93.0%, 82.5% and 15.5% reduction in *PtrCCR2* transcript abundance (Fig. 7a), respectively, were selected for further analysis. Among the three lines, the plant growth of i26-4 was affected, with a half-height compared with the wild-type, and i26-4 showed a very weak coloration on the xylem. Consistent with transcript reduction, the PtrCCR2 protein abundance was reduced in these RNAi lines, with the largest reduction of 91.4% in i26-4 (Fig. 7b). The SDX CCR enzyme activity for conversion of feruloyl-CoA to coniferaldehyde was also reduced in i26-4 by 51.5% (Fig. 7c). The 51.5% reduction in SDX CCR activity may explain why the xylem coloration in i26-4 is not as strong as described previously in *CCR* antisense poplar transgenics (Leple *et al.*, 2007). We further tested the SDX CAD activity. The CAD activities using both substrates, coniferaldehyde and sinapaldehyde, were reduced by 36.4% and 38.8%, respectively, in i26-4 (Fig. 7d; Table S7). Pearson correlation and linear regression analyses of each of the enzyme activities with CCR activities were performed in *PtrCCR2* RNAi transgenics, as in *PtrCAD1* RNAi transgenics (Tables S8, S9). Among the three families, HCT and CAD activities had positive correlations with CCR activities (Table S9). The PtrCAD1 protein levels in the three *PtrCCR2* RNAi lines were not significantly different from those in the wild-type (Fig. 7e). These results show that suppression of *PtrCCR2* gene

© 2018 The Authors
New Phytologist © 2018 New Phytologist Trust

14698137, 2019, 1, Downloaded from https://nph.onlinelibrary.wiley.com/doi/10.1111/nph.15505 by CochraneChina, Wiley Online Library on [31/01/2024]. See the Terms and Conditions (https://onlinelibrary.wiley.com/terms-and-conditions) on Wiley Online Library for rules of use; OA articles are governed by the applicable Creative Commons License

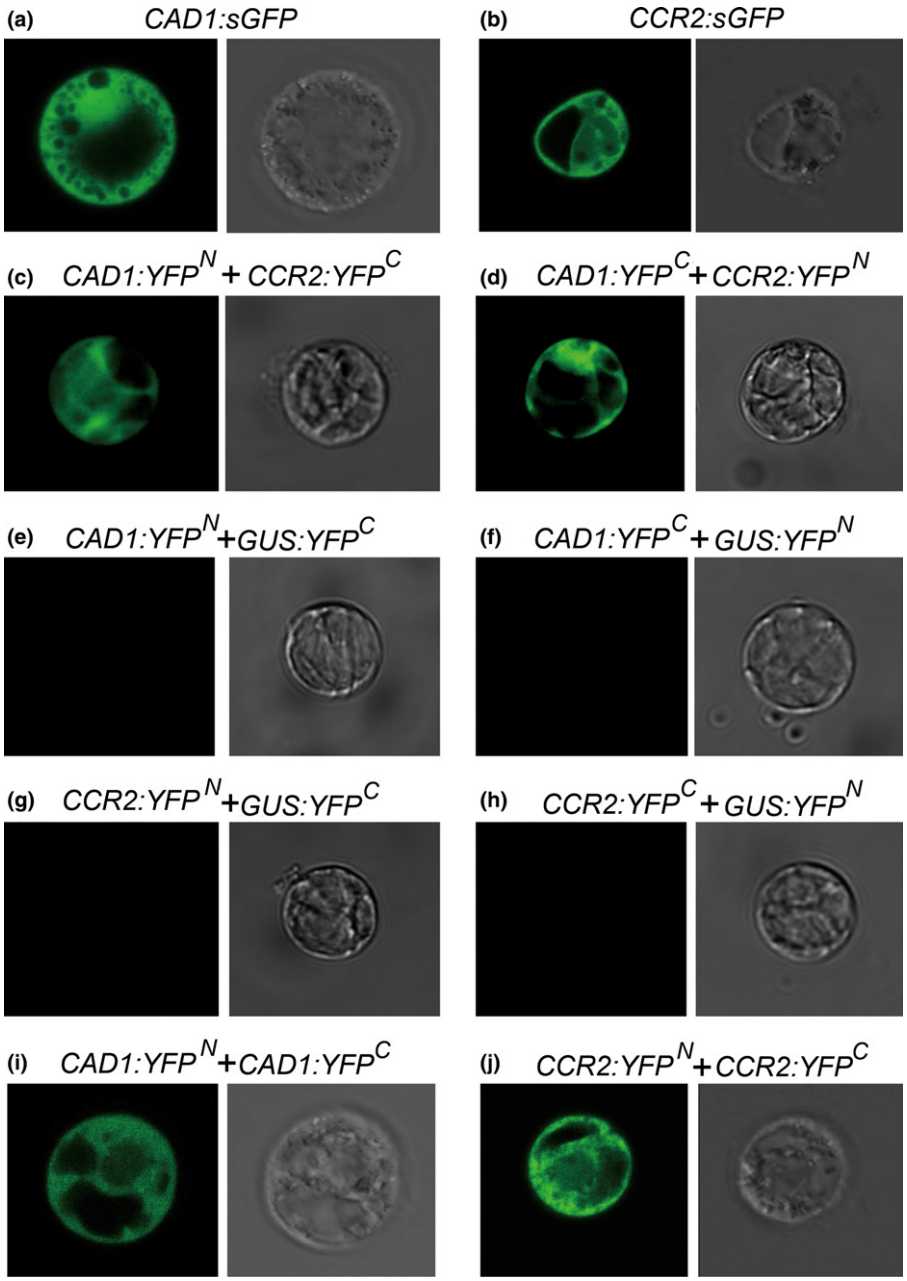

Fig. 5 Bimolecular fluorescence complementation (BiFC) assays in *Populus trichocarpa* stem-differentiating xylem (SDX) protoplasts demonstrate the homodimeric and heterodimeric formation of PtrCAD1 and PtrCCR2. (a, b) Subcellular localizations of (a) PtrCAD1 and (b) PtrCCR2 in *P. trichocarpa* SDX protoplasts. (c) BiFC assays of *in vivo* interaction between PtrCAD1 and PtrCCR2 in *P. trichocarpa* SDX protoplasts, which were cotransfected with *PtrCAD1:EYFP*^{N} and *PtrCCR2:EYFP*^{C}. (d) BiFC assays of PtrCAD1 and PtrCCR2 interaction in SDX protoplasts which were cotransfected with *PtrCAD1:EYFP*^{C} and *PtrCCR2:EYFP*^{N}. (e–h) Negative controls of BiFC assays. SDX protoplasts were cotransfected with (e) *PtrCAD1:EYFP*^{N} and *GUS:EYFP*^{C}, (f) *PtrCAD1:EYFP*^{C} and *GUS:EYFP*^{N}, (g) *PtrCCR2:EYFP*^{N} and *GUS:EYFP*^{C}, and (h) *PtrCCR2:EYFP*^{C} and *GUS:EYFP*^{N}. (i) BiFC assays of PtrCAD1 homodimer formation. Protoplasts were cotransfected with *PtrCAD1:EYFP*^{N} and *PtrCAD1:EYFP*^{C}. (j) BiFC assays of PtrCCR2 homodimer formation. Protoplasts were cotransfected with *PtrCCR2:EYFP*^{N} and *PtrCCR2:EYFP*^{C}.

expression did not affect the PtrCAD1 protein level, but caused a reduction in SDX CAD enzyme activity.

In the three selected transgenic lines, i26-4, i26-9 and i26-10, the lignin content was reduced by 32.5%, 12.9% and 11.0%, respectively (Table 1). The cellulose content was reduced and the arabinan content was significantly increased in all three lines (Table 1). Significant reductions were observed in mannan and galactan + rhamnan contents. The wood composition changes in i33 and i26 exhibited the same patterns, with an increase in arabinan content and a decrease in other components, indicating that the downregulation of *PtrCAD1* and *PtrCCR2* caused the same effects on cell wall composition. The mechanism of how lignin reduction causes changes in polysaccharide contents requires further study.

NMR spectroscopy was used to analyze lines i26-4 and i26-9. An obvious increase in ferulic acid incorporated into lignin was

© 2018 The Authors
New Phytologist © 2018 New Phytologist Trust

14698137, 2019, 1, Downloaded from https://nph.onlinelibrary.wiley.com/doi/10.1111/nph.15505 by CochraneChina, Wiley Online Library on [31/01/2024]. See the Terms and Conditions (https://onlinelibrary.wiley.com/terms-and-conditions) on Wiley Online Library for rules of use; OA articles are governed by the applicable Creative Commons License

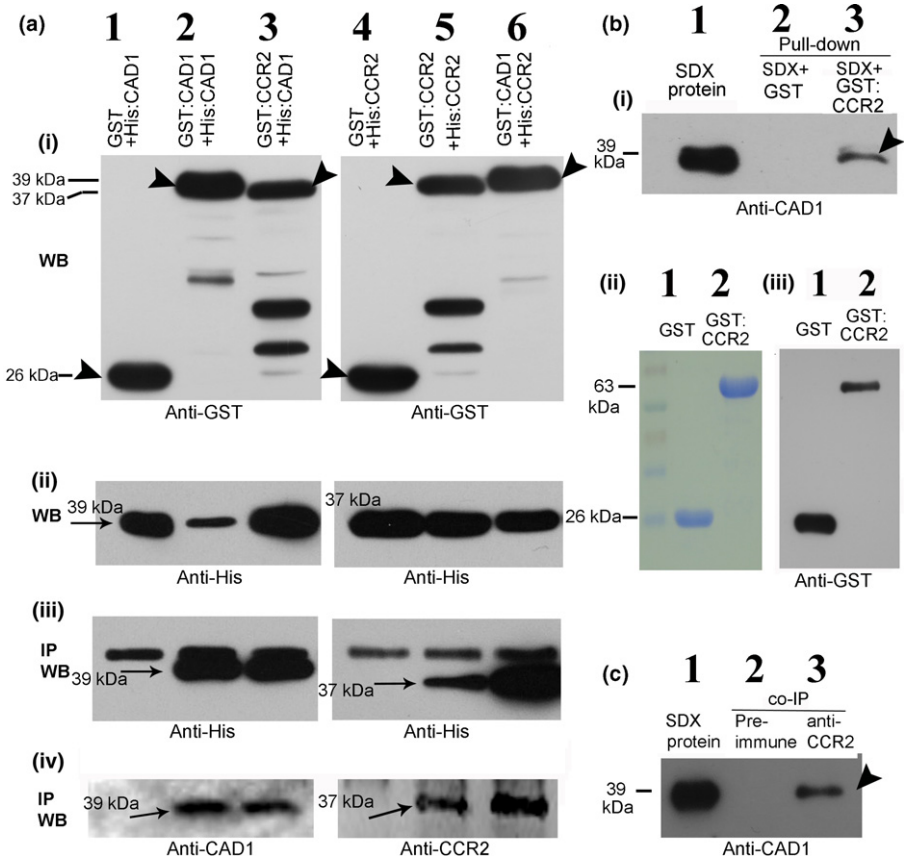

Fig. 6 Interactions of PtrCAD1 and PtrCCR2 by pull-down and co-immunoprecipitation (Co-IP). (a) Pull-down assays in *Escherichia coli* BL21 (DE3) cells. Histidine (His)-tagged and glutathione *S*-transferase (GST)-tagged proteins were coexpressed in *E. coli*. Crude proteins were immunoprecipitated by anti-GST antibodies and western blotting was conducted using anti-His antibodies and anti-CAD1/CCR2 antibodies. The expression of GST-tagged proteins and His-tagged proteins in *E. coli* was identified by western blotting with (a-i) anti-GST antibodies and (a-ii) anti-His antibodies. Immunoprecipitated proteins were identified by (a-iii) anti-His antibodies and (a-iv) anti-PtrCAD1/PtrCCR2 antibodies. Lane 1, coexpression of GST and His:PtrCAD1 in cell 1; lane 2, coexpression of GST:PtrCAD1 and His:PtrCAD1 in cell 2; lane 3, coexpression of GST:PtrCCR2 and His:PtrCAD1:His in cell 3; lane 4, coexpression of GST and His:PtrCCR2 in cell 4; lane 5, coexpression of GST:PtrCCR2 and His:PtrCCR2 in cell 5; lane 6, coexpression of GST:PtrCAD1 and His:PtrCCR2 in cell 6. Western blotting was carried out with the total proteins from the six types of cell with anti-GST antibodies and anti-His antibodies. (a-i) Western blotting for detection of GST-fused proteins. The arrowheads denote the expression of GST in cell 1 (lane 1), GST:PtrCAD1 in cell 2 (lane 2), GST:PtrCCR2 in cell 3 (lane 3), GST in cell 4 (lane 4), GST:PtrCCR2 in cell 5 (lane 5) and GST:PtrCAD1 in cell 6 (lane 6). Other bands in the immunoblot may be a result of nonspecific binding. (a-ii) Western blotting for detection of His-tagged proteins. The arrows show the expression of His:PtrCAD1 in cells 1, 2 and 3 (lanes 1, 2 and 3), and the expression of His:PtrCCR2 in cells 4, 5 and 6 (lanes 4, 5 and 6). (a-iii) Total protein extracts from the six types of cell above were immunoprecipitated with anti-GST antibodies and the immunoprecipitated proteins were detected by western blotting with anti-His antibodies. His: PtrCAD1 was pulled down by anti-GST antibodies from cells 2 and 3 (lanes 2 and 3), and His:PtrCCR2 was pulled down by anti-GST antibodies from cells 5 and 6 (lanes 5 and 6). The arrows denote the co-immunoprecipitated His:PtrCAD1 (lanes 2 and 3) and His: PtrCCR2 (lanes 5 and 6). The upper band present in all six lines may be a result of nonspecific binding of the beads and the size is larger than predicted. (a-iv) Western blotting with anti-PtrCAD1 antibodies (lanes 1–3) and with anti-PtrCCR2 antibodies (lanes 4–6). Arrows show the immunoprecipitated PtrCAD1 (lanes 2 and 3) and PtrCCR2 (lanes 5 and 6). IP, immunoprecipitation; WB, western blotting. (b) Pull-down assays in *Populus trichocarpa* stem-differentiating xylem (SDX). (b-i) Lane 1, western blotting by anti-PtrCAD1 antibodies with SDX proteins loaded as input; lane 2, SDX proteins were incubated with GST, purified by glutathione-*S*-agarose beads and probed with anti-PtrCAD1 antibodies; no signal was observed; lane 3, SDX proteins were incubated with GST:PtrCCR2 fusion proteins, purified by glutathione-*S*-agarose beads and probed with anti-PtrCAD1 antibodies. The arrowhead denotes the PtrCAD1 protein pulled down by GST:PtrCCR2 fusion proteins and glutathione-*S*-agarose beads. (b-ii) Coomassie blue-stained gels of purified GST (lane 1) and GST:PtrCCR2 (lane 2) that were added to SDX above. (b-iii) The purified products in (b-i) were probed with anti-GST antibodies. Lane 1, the band represents the GST proteins. Lane 2, the band represents the GST:PtrCCR2 fusion proteins. (c) Co-IP in *P. trichocarpa* SDX. SDX proteins were immunoprecipitated with anti-PtrCCR2 antibodies, and immunoprecipitated proteins were detected by anti-PtrCAD1 antibodies. SDX proteins were loaded as an input (lane 1). Preimmune serum was used as the control (lane 2). Arrowhead (lane 3) denotes the signal of detected PtrCAD1.

observed in i26-4 (Fig. 8). The NMR results also indicated the concomitant downregulation of *PtrCCR2*, because lignin-bound ferulic acid is an indicator of CCR deficiency, with the bis-ferulate ether (ferulic acid marker) being a particularly diagnostic marker (Ralph *et al.*, 2008).

Enzyme activities with a mixture of PtrCAD1 and PtrCCR2 recombinant proteins support their interactions

To understand the allosteric effects of PtrCAD1 and PtrCCR2 interactions, we mixed these two *E. coli* recombinant proteins at

© 2018 The Authors
New Phytologist © 2018 New Phytologist Trust

14698137, 2019, 1, Downloaded from https://nph.onlinelibrary.wiley.com/doi/10.1111/nph.15505 by CochraneChina, Wiley Online Library on [31/01/2024]. See the Terms and Conditions (https://onlinelibrary.wiley.com/terms-and-conditions) on Wiley Online Library for rules of use; OA articles are governed by the applicable Creative Commons License

14698137, 2019, 1, Downloaded from https://nph.onlinelibrary.wiley.com/doi/10.1111/nph.15505 by CochraneChina, Wiley Online Library on [31/01/2024]. See the Terms and Conditions (https://onlinelibrary.wiley.com/terms-and-conditions) on Wiley Online Library for rules of use; OA articles are governed by the applicable Creative Commons License

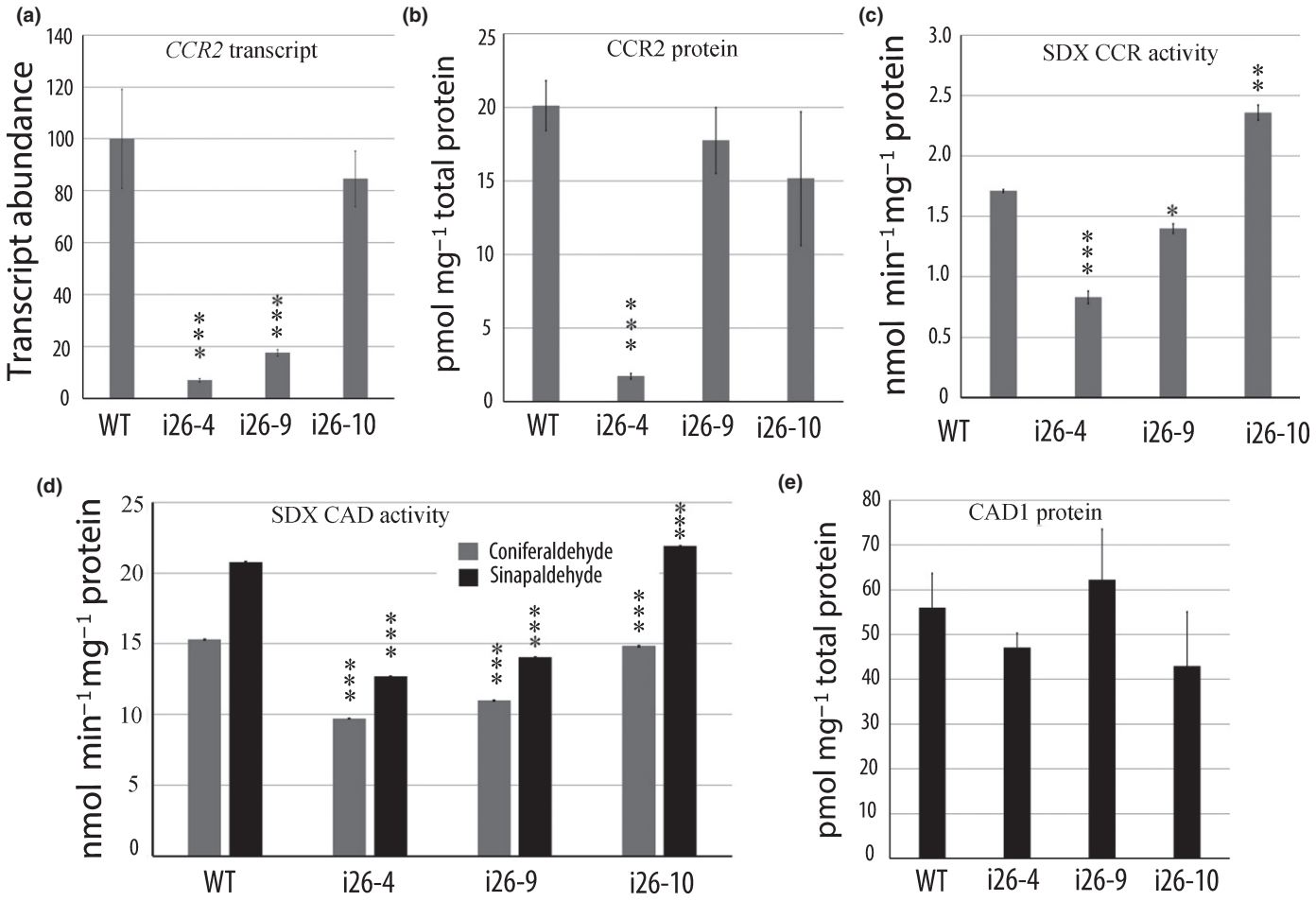

Fig. 7 Downregulation of *PtrCCR2* in the *Populus trichocarpa* stem-differentiating xylem (SDX) of RNAi knockdown transgenics. (a) *PtrCCR2* transcript abundance in the three *PtrCCR2* knockdown transgenic lines (i26-4, i26-9 and i26-10) and wild-type (WT). (b) Protein quantification of PtrCCR2 in *PtrCCR2* knockdown transgenics. (c) SDX protein cinnamoyl-CoA reductase (CCR) activities of conversion of feruloyl-CoA to coniferaldehyde. (d) Enzyme activities of the SDX cinnamyl alcohol dehydrogenase (CAD) family in *PtrCCR2* knockdown transgenic plants. Gray bars represent the SDX enzyme activities of conversion of coniferyl aldehyde to coniferyl alcohol. Black bars represent the SDX enzyme activities of conversion of sinapaldehyde to sinapyl alcohol. (e) Protein quantification of PtrCAD1 in *PtrCCR2* knockdown transgenics. Errors bars represent ±SE of three biological replicates. Asterisks highlight significant differences by Student's *t*-test: *, $P < 0.05$; **, $P < 0.01$; ***, $P < 0.001$.

different molar ratios and conducted enzyme assays to determine whether the enzyme activities were affected. Considering that feruloyl-CoA can be successively converted to coniferaldehyde by CCR and to coniferyl alcohol by CAD, it is difficult to determine CCR activities in the mixed enzyme assays. We only examined the effects on CAD activities by PtrCAD1 and PtrCCR2 interactions. In the mixed enzyme assay, PtrCAD1 was kept at a fixed concentration of 20 nM, and PtrCCR2 was added at concentrations of 10, 20, 40, 60, 80 and 100 nM, respectively. When the concentration of added PtrCCR2 was increased, the rate of conversion of coniferaldehyde to coniferyl alcohol was increased, and PtrCAD1 activities with PtrCCR2 added were significantly higher than the control with the same concentration of BSA added (Fig. 9a). However, compared with control with BSA added, PtrCAD1 activities of conversion of sinapaldehyde to sinapyl alcohol with PtrCCR2 added showed no significant difference (Fig. 9b). Furthermore, we conducted enzyme assays using coexpressed proteins. Compared with the crude protein extracts with PtrCAD1/GST coexpressed, PtrCAD1 activities of PtrCAD1/PtrCCR2-coexpressed crude proteins, using both coniferaldehyde and sinapaldehyde as substrates, were significantly increased (Fig. 9c), supporting the interaction of PtrCAD1 and PtrCCR2.

Discussion

Proteins are major components within an organism, performing a vast array of biological functions. Proteins rarely act alone. They form complexes, providing a level of protein function regulation. Complex formation has been implicated in the phenylpropanoid and flavonoid biosynthetic pathways (Winkel-Shirley, 1999; Chen *et al.*, 2011, 2014). It has been proposed that multi-enzymes catalyze sequential reactions for phenylpropanoid biosynthesis (Winkel-Shirley, 1999). Early indications came from the study of the enzymes PAL and C4H, which catalyze the first two steps of the phenylpropanoid pathway (Czichi & Kindl, 1977; Hrazdina

© 2018 The Authors
New Phytologist © 2018 New Phytologist Trust

New Phytologist

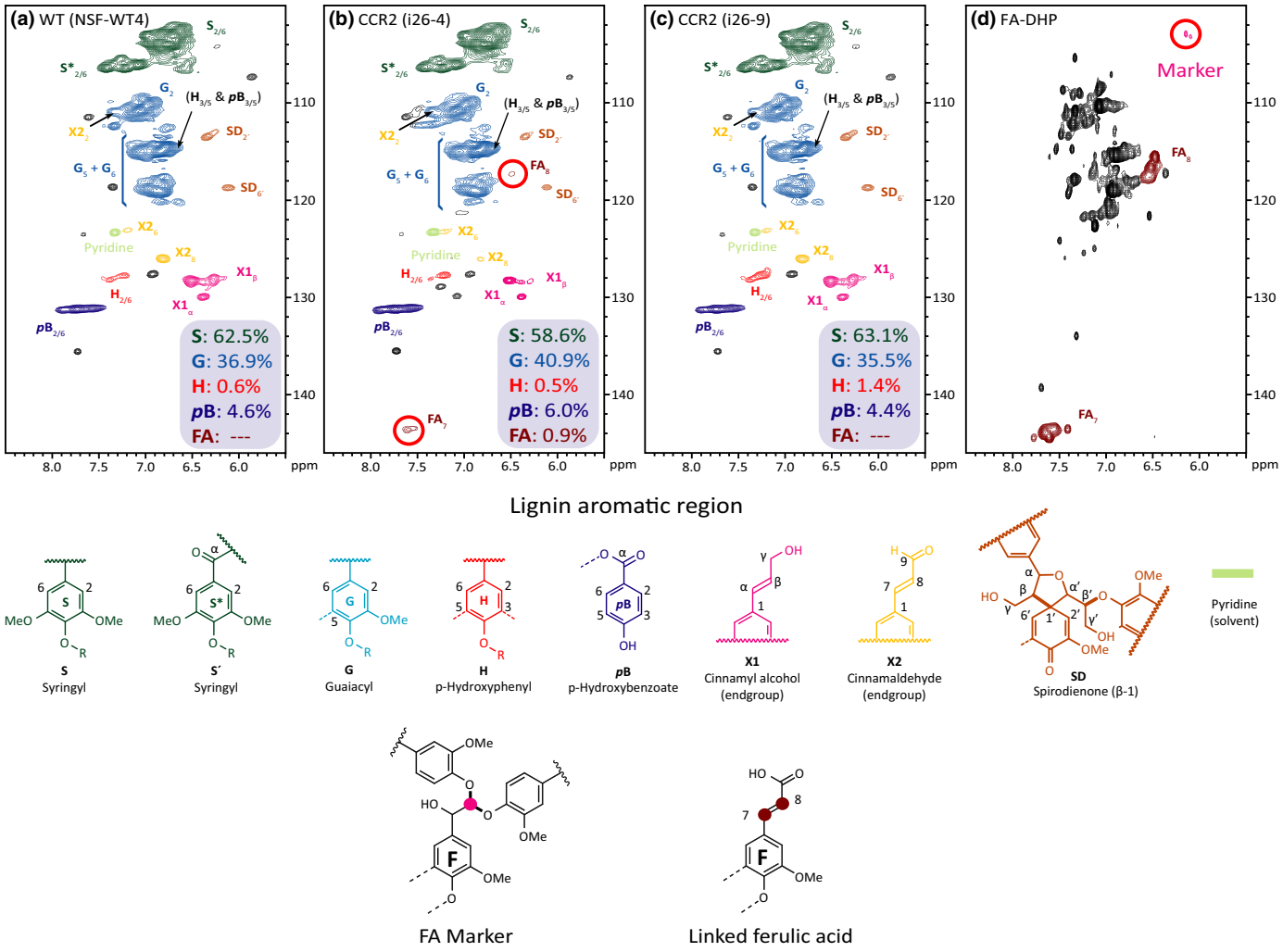

Fig. 8 Heteronuclear single-quantum coherence (HSQC) nuclear magnetic resonance (NMR) spectra of cellulolytic enzyme lignins (CELs) from *Populus trichocarpa CCR2* (*PtrCCR2*) knockdown transgenic wood shows the lignin aromatic region of (a) wild-type (WT), (b) i26-4, (c) i263-9 and (d) Ferulic acid (FA) marker.

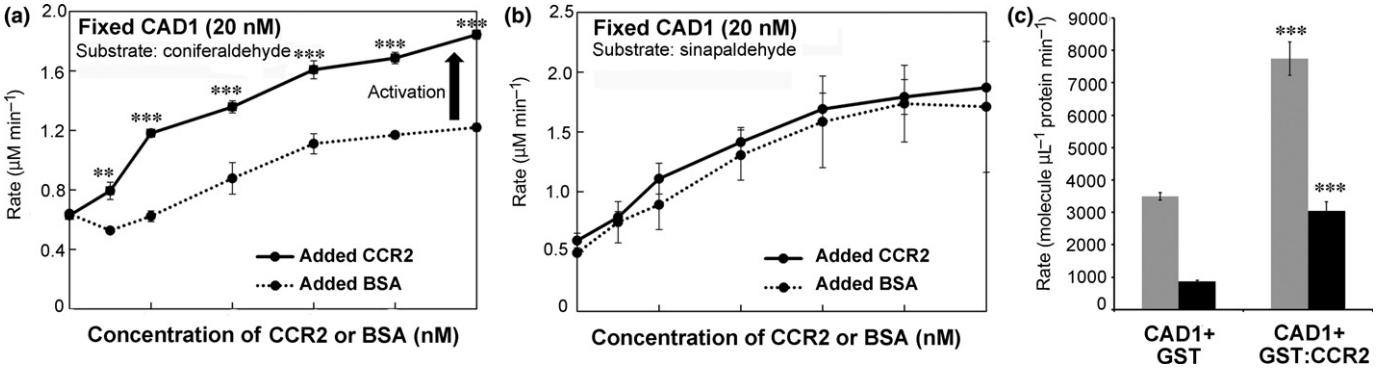

Fig. 9 Impact of PtrCAD1 and PtrCCR2 interactions on enzyme activity. (a, b) Enzyme assays using mixed recombinant proteins. Cinnamyl alcohol dehydrogenase (CAD) activity was assayed by fixing the PtrCAD1 concentration at 20 nM, whilst varying the PtrCCR2 concentration from 0 to 100 nM, using 50 μM of (a) coniferaldehyde or (b) sinapaldehyde as the substrate. The CAD activity changes are shown as solid lines. Bovine serum albumin (BSA) controls (dashed lines) represent assays with the addition of BSA (a noninteracting protein) instead of the interacting protein (i.e. mixing PtrCAD1 with BSA instead of PtrCCR2). The arrows indicate the activation impacts by protein–protein interactions. (c) Enzyme assays using coexpressed proteins. One crude protein contained coexpressed His:PtrCAD1 and GST (CAD1 + GST), and the other crude protein contained coexpressed His:PtrCAD1 and GST:PtrCCR2 (CAD1 + GST:CCR2). The two crude proteins had the same PtCAD1 protein abundance, identified by western blotting using anti-His antibodies (data not shown). Gray bars represent CAD activities using coniferaldehyde as substrate. Black bars represent CAD activities using sinapaldehyde as substrate. Error bars represent 1 ± SE of three technical replicates. In some cases, the precision is high, and the error bars are smaller than the size of the data points. Asterisks highlight significant differences by Student's *t*-test: **, $P < 0.01$; ***, $P < 0.001$.

© 2018 The Authors
New Phytologist © 2018 New Phytologist Trust

14698137, 2019, 1, Downloaded from https://nph.onlinelibrary.wiley.com/doi/10.1111/nph.15505 by CochraneChina, Wiley Online Library on [31/01/2024]. See the Terms and Conditions (https://onlinelibrary.wiley.com/terms-and-conditions) on Wiley Online Library for rules of use; OA articles are governed by the applicable Creative Commons License

14698137, 2019, 1, Downloaded from https://nph.onlinelibrary.wiley.com/doi/10.1111/nph.15505 by CochraneChina, Wiley Online Library on [31/01/2024]. See the Terms and Conditions (https://onlinelibrary.wiley.com/terms-and-conditions) on Wiley Online Library for rules of use; OA articles are governed by the applicable Creative Commons License

& Wagner, 1985). Isolated microsomes preferentially convert phenylalanine to *p*-coumaric acid rather than cinnamic acid to *p*-coumaric acid. When microsomes were gently homogenized, cinnamic acid could be efficiently converted to *p*-coumarate (Hrazdina & Wagner, 1985). These results indicate that PAL and C4H activities are coupled and the proteins are closely associated. Furthermore, PAL and C4H were found to be colocalized in the membrane, and C4H may serve to organize the complex for membrane association of PAL (Achnine *et al.*, 2004). Similarly, two other soluble proteins, HCT and 4CL, were found to be relocalized to the membrane on C3H and/or C4H expression (Bassard *et al.*, 2012). It has been proposed that C3H and C4H form complexes, localized in the endoplasmic reticulum (Chen *et al.*, 2011; Bassard *et al.*, 2012). C3H and C4H could both enable the association of soluble proteins PAL, HCT and 4CL to the membrane, but it appears that C3H plays a more prominent nucleation role (Bassard *et al.*, 2012). To date, evidence showing that PAL, HCT and 4CL are organized into C3H/C4H complexes is lacking. In this study, we found that two soluble proteins, CAD and CCR, which catalyze the last two steps of monolignol biosynthesis, interact with each other. The evidence for PtrCAD1/PtrCCR2 protein complex formation includes BiFC, pull-down/Co-IP and mixed enzyme assays. In the transgenics with one gene of *PtrCAD1* and *PtrCCR2* suppressed, the SDX activity of the other family is reduced, supporting their interaction. Although the enzyme activities of some other families in monolignol biosynthesis were affected in the transgenics (Tables S2, S7), only CAD activity and CCR activity show positive correlations in both *PtrCAD1* and *PtrCCR2* RNAi transgenics (Tables S3–S6, S8, S9). HCT activity also shows positive correlations with CCR activity in *PtrCCR2* RNAi transgenics. Whether PtrCAD1 and PtrCCR2 form complexes with membrane proteins through HCT as a bridge requires further investigation. Our recent observations suggest that further enzymes in monolignol biosynthesis show interactions and they may form a larger complex. We are using additional approaches, including pull-down/LC-MS, to carry out a deeper study of the protein complexes in monolignol biosynthesis.

Physical contact between proteins often results in activation or repression of the enzyme activities of the participating proteins. The binding of one enzyme to another could induce conformational changes that affect enzyme activity or binding ability to substrates. *In vitro* enzyme kinetics revealed that PtrC4H1/C4H2/C3H complexes showed increased activities of individual enzymes for the 4-hydroxylation of cinnamic acid and 3-hydroxylation of *p*-coumaroyl shikimic acid, but also showed drastically increased enzyme metabolic efficiency (increased V_{max}/K_m values) on *p*-coumaric acid, indicating the involvement of the complex in the 3-hydroxylation of *p*-coumaric acid (Chen *et al.*, 2011). Two 4CL isomers, Ptr4CL3 and Ptr4CL5, form complexes, in which Ptr4CL5 may play a regulatory role, affecting the kinetic behavior of Ptr4CL3. In this case, 4CL substrate specificity is affected, facilitating the CoA ligation of both *p*-coumaric acid and caffeic acid for monolignol biosynthesis (Chen *et al.*, 2014). In this study, we observed a reduction in CCR activity in transgenic SDX with reduced PtrCAD1 protein quantity, and also observed a reduction in CAD activity in transgenic SDX with reduced PtrCCR2 protein quantity, indicating that the reduction in activity may be caused by the disruption of PtrCAD1 and PtrCCR2 interaction.

In comparison, PtrCAD1/PtrCCR2 heterodimers have a higher activity than homodimers. Heterodimers may have different substrate affinities relative to homodimers because of conformational changes, which requires further study. It would be interesting to examine the ratio of PtrCAD1 : PtrCCR2 homodimers and heterodimers within the plants. Heterodimers may be formed under certain conditions to increase enzyme activity. The complexity of monolignol biosynthesis and its regulation may be a result of adaptation, such as environmental stresses. Protein–protein interaction is required for the stress-induced synthesis of 5-deoxy flavonoid derivatives (Dixon & Paiva, 1995). The mechanisms regulating complex formation in monolignol biosynthesis remain unclear. Moreover, PtrCAD1 activities using both coniferaldehyde and sinapaldehyde as substrates were increased when the proteins were coexpressed. However, when we mixed PtrCAD1 and PtrCCR2 for CAD enzyme assays, we observed an increased PtrCAD1 activity for the conversion of coniferaldehyde to coniferyl alcohol, but not for PtrCAD1 activity for the conversion of sinapaldehyde to sinapyl alcohol. Possibly, the optimum conditions for PtrCAD1 activity on sinapaldehyde may be different from those *in vivo*, or an additional component may be needed for the conversion of sinapaldehyde to sinapyl alcohol. PtrCAD1–PtrCCR2 interactions may be different for G and S monolignol biosynthesis. In a recent study of poplar (*P. tremula* × *alba*) *CAD1* silencing transgenics with a 95% reduction in *CAD1* transcript abundance, only sinapaldehyde, but not coniferaldehyde, was incorporated at increased levels into the lignin polymer (Acker *et al.*, 2017). The difference in PtrCAD1–PtrCCR2 interactions between CAD activities on coniferaldehyde and sinapaldehyde may cause the sequestration of coniferaldehyde in a more efficient way than sinapaldehyde, and coniferaldehyde is converted into ferulic acid and derivatives in the *CAD1* transgenics. Further experiments are needed to elucidate the mechanism of selective incorporation of aldehyde into the lignin polymer in the CAD1-silenced transgenics.

Monolignol biosynthesis is regulated at multiple levels, including the post-translational level. Recently, phosphorylation was discovered as an on/off switch for PtrCOMT2 activity (Wang *et al.*, 2015). Protein complex formation in monolignol biosynthesis may be a more efficient way to increase enzyme activity than *de novo* gene expression on reaction to environmental stimuli. The elucidation of the regulation of monolignol biosynthesis requires a comprehensive study at the systems level, which may also help in the design of strategies for the engineering of lignin to improve plant growth and adaptation.

Acknowledgements

This work was supported by grants from the Fundamental Research Funds of CAF (CAFYBB2016ZX001-1), the National

© 2018 The Authors
New Phytologist © 2018 New Phytologist Trust

Key Research and Development Program of China (2016YFD0600103) and the National Science Foundation Plant Genome Research Program Grant (DBI-0922391). HK and JR (and the NMR instrumentation used in this work) were partially funded by the DOE Great Lakes Bioenergy Research Center (DOE Office of Science BER DE-FC02-07ER64494 and DE-SC0018409).

Author contributions

QL and VLC designed the experiments. XY, JL, HK, BL, XH, ZY, Y-CL, HC, CY, JPW and QL performed the experiments. XY, HK, DCM, JR, RRS, QL and VLC analyzed the data, and XY, HK, JR, RRS and QL wrote the manuscript. XY, JL, HK and BL contributed equally to this work.

References

Achnine L, Blancaflor EB, Rasmussen S, Dixon RA. 2004. Colocalization of L-phenylalanine ammonia-lyase and cinnamate 4-hydroxylase for metabolic channeling in phenylpropanoid biosynthesis. *Plant Cell* **16**: 3098–3109.

Acker RV, Déjardin A, Desmet S, Hoengenaert L, Vanholme R, Morreel K, Laurans F, Kim H, Santoro N, Foster C. 2017. Different routes for conifer- and sinapaldehyde and higher saccharification upon deficiency in the dehydrogenase CAD1. *Plant Physiology* **175**: 1018.

Bassard J-E, Richert L, Geerinck J, Renault H, Duval F, Ullmann P, Schmitt M, Meyer E, Mutterer J, Boerjan W. 2012. Protein–protein and protein–membrane associations in the lignin pathway. *Plant Cell* **24**: 4465–4482.

Baucher M, Chabbert B, Pilate G, Van Doorsselaere J, Tollier M-T, Petit-Conil M, Cornu D, Monties B, Van Montagu M, Inze D. 1996. Red xylem and higher lignin extractability by down-regulating a cinnamyl alcohol dehydrogenase in poplar. *Plant Physiology* **112**: 1479–1490.

Berthet S, Demont-Caulet N, Pollet B, Bidzinski P, Cézard L, Le Bris P, Borrega N, Hervé J, Blondet E, Balzergue S *et al.* 2011. Disruption of *LACCASE4* and *17* results in tissue-specific alterations to lignification of *Arabidopsis thaliana* stems. *Plant Cell* **23**: 1124–1137.

Boerjan W, Ralph J, Baucher M. 2003. Lignin biosynthesis. *Annual Review of Plant Biology* **54**: 519–546.

Bouvier d'Yvoire M, Bouchabke-Coussa O, Voorend W, Antelme S, Cézard L, Legée F, Lebris P, Legay S, Whitehead C, McQueen-Mason SJ. 2013. Disrupting the *cinnamyl alcohol dehydrogenase 1* gene (*BdCAD1*) leads to altered lignification and improved saccharification in *Brachypodium distachyon*. *Plant Journal* **73**: 496–508.

Chen F, Dixon RA. 2007. Lignin modification improves fermentable sugar yields for biofuel production. *Nature Biotechnology* **25**: 759–761.

Chen H-C, Li Q, Shuford CM, Liu J, Muddiman DC, Sederoff RR, Chiang VL. 2011. Membrane protein complexes catalyze both 4- and 3-hydroxylation of cinnamic acid derivatives in monolignol biosynthesis. *Proceedings of the National Academy of Sciences, USA* **108**: 21253–21258.

Chen H-C, Song J, Wang JP, Lin Y-C, Ducoste J, Shuford CM, Liu J, Li Q, Shi R, Nepomuceno A. 2014. Systems biology of lignin biosynthesis in *Populus trichocarpa*: heteromeric 4-coumaric acid:coenzyme A ligase protein complex formation, regulation, and numerical modeling. *Plant Cell* **26**: 876–893.

Czichi U, Kindl H. 1977. Phenylalanine ammonia lyase and cinnamic acid hydroxylases as assembled consecutive enzymes on microsomal membranes of cucumber cotyledons: cooperation and subcellular distribution. *Planta* **134**: 133–143.

Dixon R, Achnine L, Deavours B, Naoumkina M. 2006. Metabolomics and gene identification in plant natural product pathways. In: Saito K, Dixon RA, Willmitzer L, eds. *Plant metabolomics*. Berlin, Germany: Springer-Verlag, 243–259.

Dixon RA, Chen F, Guo D, Parvathi K. 2001. The biosynthesis of monolignols: a "metabolic grid", or independent pathways to guaiacyl and syringyl units? *Phytochemistry* **57**: 1069–1084.

Dixon RA, Paiva NL. 1995. Stress-induced phenylpropanoid metabolism. *Plant Cell* **7**: 1085.

Freudenberg K, Neish AC. 1968. *Constitution and biosynthesis of lignin*. New York, NY, USA: Springer-Verlag.

Gallego-Giraldo L, Escamilla-Trevino L, Jackson LA, Dixon RA. 2011. Salicylic acid mediates the reduced growth of lignin down-regulated plants. *Proceedings of the National Academy of Sciences, USA* **108**: 20814–20819.

Halpin C, Holt K, Chojecki J, Oliver D, Chabbert B, Monties B, Edwards K, Barakate A, Foxon GA. 1998. Brown-midrib maize (bm1)–a mutation affecting the cinnamyl alcohol dehydrogenase gene. *Plant Journal* **14**: 545–553.

Higuchi T. 2003. Pathways for monolignol biosynthesis via metabolic grids: coniferyl aldehyde 5-hydroxylase, a possible key enzyme in angiosperm syringyl lignin biosynthesis. *Proceedings of the Japan Academy, Series B* **79**: 227–236.

Higuchi T. 2009. *Biochemistry and molecular biology of wood*. London, UK: Oxford University Press.

Hrazdina G, Wagner GJ. 1985. Metabolic pathways as enzyme complexes: evidence for the synthesis of phenylpropanoids and flavonoids on membrane associated enzyme complexes. *Archives of Biochemistry and Biophysics* **237**: 88–100.

Hu W-J, Harding SA, Lung J, Popko JL, Ralph J, Stokke DD, Tsai C-J, Chiang VL. 1999. Repression of lignin biosynthesis promotes cellulose accumulation and growth in transgenic trees. *Nature Biotechnology* **17**: 808–812.

Karlen SD, Zhang C, Peck ML, Smith RA, Padmakshan D, Helmich KE, Free HC, Lee S, Smith BG, Lu F. 2016. Monolignol ferulate conjugates are naturally incorporated into plant lignins. *Science Advances* **2**: e1600393.

Kim H, Ralph J, Lu F, Ralph SA, Boudet A-M, MacKay JJ, Sederoff RR, Ito T, Kawai S, Ohashi H *et al.* 2003. NMR analysis of lignins in CAD-deficient plants. Part 1. Incorporation of hydroxycinnamaldehydes and hydroxybenzaldehydes into lignins. *Organic & Biomolecular Chemistry* **1**: 268–281.

Kim H, Ralph J, Yahiaoui N, Pean M, Boudet A-M. 2000. Cross-coupling of hydroxycinnamyl aldehydes into lignins. *Organic Letters* **2**: 2197–2200.

Lapierre C, Pollet B, Petit-Conil M, Toval G, Romero J, Pilate G, Leplé J-C, Boerjan W, Ferret V, De Nadai V. 1999. Structural alterations of lignins in transgenic poplars with depressed cinnamyl alcohol dehydrogenase or caffeic acid *O*-methyltransferase activity have an opposite impact on the efficiency of industrial kraft pulping. *Plant Physiology* **119**: 153–164.

Leple J-C, Dauwe R, Morreel K, Storme V, Lapierre C, Pollet B, Naumann A, Kang K-Y, Kim H, Ruel K. 2007. Downregulation of cinnamoyl-coenzyme A reductase in poplar: multiple-level phenotyping reveals effects on cell wall polymer metabolism and structure. *Plant Cell* **19**: 3669–3691.

Li L, Cheng X, Lu S, Nakatsubo T, Umezawa T, Chiang VL. 2005. Clarification of cinnamoyl co-enzyme A reductase catalysis in monolignol biosynthesis of aspen. *Plant and Cell Physiology* **46**: 1073–1082.

Li Q, Lin Y-C, Sun Y-H, Song J, Chen H, Zhang X-H, Sederoff RR, Chiang VL. 2012. Splice variant of the SND1 transcription factor is a dominant negative of SND1 members and their regulation in *Populus trichocarpa*. *Proceedings of the National Academy of Sciences, USA* **109**: 14699–14704.

Li Q, Min D, Wang JP-Y, Peszlen I, Horvath L, Horvath B, Nishimura Y, Jameel H, Chang H-M, Chiang VL. 2011. Down-regulation of glycosyltransferase 8D genes in *Populus trichocarpa* caused reduced mechanical strength and xylan content in wood. *Tree Physiology* **31**: 226–236.

Li Q, Song J, Peng S, Wang JP, Qu GZ, Sederoff RR, Chiang VL. 2014. Plant biotechnology for lignocellulosic biofuel production. *Plant Biotechnology Journal* **12**: 1174–1192.

Lin Y-C, Li W, Chen H, Li Q, Sun Y-H, Shi R, Lin C-Y, Wang JP, Chen H-C, Chuang L *et al.* 2014. A simple improved-throughput xylem protoplast system for studying wood formation. *Natural Protocol* **9**: 2194–2205.

Liu J, Shi R, Li Q, Sederoff RR, Chiang VL. 2012. A standard reaction condition and a single HPLC separation system are sufficient for estimation of monolignol biosynthetic pathway enzyme activities. *Planta* **236**: 879–885.

© 2018 The Authors
New Phytologist © 2018 New Phytologist Trust

14698137, 2019, 1, Downloaded from https://nph.onlinelibrary.wiley.com/doi/10.1111/nph.15505 by CochraneChina, Wiley Online Library on [31/01/2024]. See the Terms and Conditions (https://onlinelibrary.wiley.com/terms-and-conditions) on Wiley Online Library for rules of use; OA articles are governed by the applicable Creative Commons License

Lu S, Li Q, Wei H, Chang M-J, Tunlaya-Anukit S, Kim H, Liu J, Song J, Sun Y-H, Yuan L. 2013. Ptr-miR397a is a negative regulator of laccase genes affecting lignin content in *Populus trichocarpa*. *Proceedings of the National Academy of Sciences, USA* **110**: 10848–10853.

MacKay JJ, O'Malley DM, Presnell T, Booker FL, Campbell MM, Whetten RW, Sederoff RR. 1997. Inheritance, gene expression, and lignin characterization in a mutant pine deficient in cinnamyl alcohol dehydrogenase. *Proceedings of the National Academy of Sciences, USA* **94**: 8255–8260.

Nakagawa T, Kurose T, Hino T, Tanaka K, Kawamukai M, Niwa Y, Toyooka K, Matsuoka K, Jinbo T, Kimura T. 2007. Development of series of gateway binary vectors, pGWBs, for realizing efficient construction of fusion genes for plant transformation. *Journal of Bioscience and Bioengineering* **104**: 34–41.

Öhman D, Demedts B, Kumar M, Gerber L, Gorzsás A, Goeminne G, Hedenström M, Ellis B, Boerjan W, Sundberg B. 2013. MYB103 is required for FERULATE-5-HYDROXYLASE expression and syringyl lignin biosynthesis in Arabidopsis stems. *Plant Journal* **73**: 63–76.

Ralph J. 2010. Hydroxycinnamates in lignification. *Phytochemistry Reviews* **9**: 65–83.

Ralph J, Kim H, Lu F, Grabber JH, Leplé JC, Berrio-Sierra J, Derikvand MM, Jouanin L, Boerjan W, Lapierre C. 2008. Identification of the structure and origin of a thioacidolysis marker compound for ferulic acid incorporation into angiosperm lignins (and an indicator for cinnamoyl CoA reductase deficiency). *Plant Journal* **53**: 368–379.

Rohde A, Morreel K, Ralph J, Goeminne G, Hostyn V, De Rycke R, Kushnir S, Van Doorsselaere J, Joseleau J-P, Vuylsteke M. 2004. Molecular phenotyping of the *pal1* and *pal2* mutants of *Arabidopsis thaliana* reveals far-reaching consequences on phenylpropanoid, amino acid, and carbohydrate metabolism. *Plant Cell* **16**: 2749–2771.

Sarkanen KV, Ludwig CH. 1971. *Lignins: occurrence, formation, structure and reactions*. New York, NY, USA: Wiley-Interscience.

Shen H, Mazarei M, Hisano H, Escamilla-Trevino L, Fu C, Pu Y, Rudis MR, Tang Y, Xiao X, Jackson L. 2013. A genomics approach to deciphering lignin biosynthesis in switchgrass. *Plant Cell* **25**: 4342–4361.

Shi R, Sun Y-H, Li Q, Heber S, Sederoff R, Chiang VL. 2010. Towards a systems approach for lignin biosynthesis in *Populus trichocarpa*: transcript abundance and specificity of the monolignol biosynthetic genes. *Plant Cell Physiology* **51**: 144–163.

Shuford CM, Li Q, Sun Y-H, Chen H-C, Wang J, Shi R, Sederoff RR, Chiang VL, Muddiman DC. 2012. Comprehensive quantification of monolignol-pathway enzymes in *Populus trichocarpa* by protein cleavage isotope dilution mass spectrometry. *Journal of Proteome Research* **11**: 3390–3404.

Song J, Lu S, Chen Z-Z, Lourenco R, Chiang VL. 2006. Genetic transformation of *Populus trichocarpa* genotype Nisqually-1: a functional genomic tool for woody plants. *Plant Cell Physiology* **47**: 1582–1589.

Timell TE. 1986. *Compression wood in gymnosperms*. New York, NY, USA: Springer-Verlag.

Tuskan GA, Difazio S, Jansson S, Bohlmann J, Grigoriev I, Hellsten U, Putnam N, Ralph S, Rombauts S, Salamov A. 2006. The genome of black cottonwood, *Populus trichocarpa* (Torr. & Gray). *Science* **313**: 1596–1604.

Umezawa T. 2010. The cinnamate/monolignol pathway. *Phytochemistry Reviews* **9**: 1–17.

Van Acker R, Vanholme R, Storme V, Mortimer JC, Dupree P, Boerjan W. 2013. Lignin biosynthesis perturbations affect secondary cell wall composition and saccharification yield in *Arabidopsis thaliana*. *Biotechnology for Biofuels* **6**: 46.

Vanholme R, Cesarino I, Rataj K, Xiao Y, Sundin L, Goeminne G, Kim H, Cross J, Morreel K, Araujo P. 2013. Caffeoyl shikimate esterase (CSE) is an enzyme in the lignin biosynthetic pathway in *Arabidopsis*. *Science* **341**: 1103–1106.

Vanholme R, Demedts B, Morreel K, Ralph J, Boerjan W. 2010. Lignin biosynthesis and structure. *Plant Physiology* **153**: 895–905.

Vanholme R, Morreel K, Ralph J, Boerjan W. 2008. Lignin engineering. *Current Opinion in Plant Biology* **11**: 278–285.

Vogt T. 2010. Phenylpropanoid biosynthesis. *Molecular Plant* **3**: 2–20.

Wang JP, Chuang L, Loziuk PL, Chen H, Lin Y-C, Shi R, Qu G-Z, Muddiman DC, Sederoff RR, Chiang VL. 2015. Phosphorylation is an on/off switch for 5-hydroxyconiferaldehyde *O*-methyltransferase activity in poplar monolignol biosynthesis. *Proceedings of the National Academy of Sciences, USA* **112**: 8481–8486.

Wang JP, Naik PP, Chen H-C, Shi R, Lin C-Y, Liu J, Shuford CM, Li Q, Sun Y-H, Tunlaya-Anukit S. 2014. Complete proteomic-based enzyme reaction and inhibition kinetics reveal how monolignol biosynthetic enzyme families affect metabolic flux and lignin in *Populus trichocarpa*. *Plant Cell* **26**: 894–914.

Weisshaar B, Jenkins GI. 1998. Phenylpropanoid biosynthesis and its regulation. *Current Opinion in Plant Biology* **1**: 251–257.

Weng JK, Chapple C. 2010. The origin and evolution of lignin biosynthesis. *New Phytologist* **187**: 273–285.

Winkel-Shirley B. 1999. Evidence for enzyme complexes in the phenylpropanoid and flavonoid pathways. *Physiologia Plantarum* **107**: 142–149.

Withers S, Lu F, Kim H, Zhu Y, Ralph J, Wilkerson CG. 2012. Identification of grass-specific enzyme that acylates monolignols with *p*-coumarate. *Journal of Biological Chemistry* **287**: 8347–8355.

Xue L-J, Guo W, Yuan Y, Anino EO, Nyamdari B, Wilson MC, Frost CJ, Chen H-Y, Babst BA, Harding SA. 2013. Constitutively elevated salicylic acid levels alter photosynthesis and oxidative state but not growth in transgenic. *Populus Plant Cell* **25**: 2714–2730.

Zhang K, Qian Q, Huang Z, Wang Y, Li M, Hong L, Zeng D, Gu M, Chu C, Cheng Z. 2006. *GOLD HULL AND INTERNODE2* encodes a primarily multifunctional cinnamyl-alcohol dehydrogenase in rice. *Plant Physiology* **140**: 972–983.

Zhao Q, Wang H, Yin Y, Xu Y, Chen F, Dixon RA. 2010. Syringyl lignin biosynthesis is directly regulated by a secondary cell wall master switch. *Proceedings of the National Academy of Sciences, USA* **107**: 14496–14501.

Zhong R, Lee C, Ye ZH. 2010. Evolutionary conservation of the transcriptional network regulating secondary cell wall biosynthesis. *Trends in Plant Science* **15**: 625–632.

Zhou J, Lee C, Zhong R, Ye ZH. 2009. MYB58 and MYB63 are transcriptional activators of the lignin biosynthetic pathway during secondary cell wall formation in *Arabidopsis*. *Plant Cell* **21**: 248–266.

Supporting Information

Additional Supporting Information may be found online in the Supporting Information section at the end of the article:

Fig. S1 Typical xylem coloration in *Populus trichocarpa CAD1* (*PtrCAD1*) RNAi transgenics.

Table S1 Primers used in this study.

Table S2 Enzyme assays of stem-differentiating xylem (SDX) proteins in *PtrCAD1* RNAi transgenics.

Table S3 Correlation analysis of each enzyme activity with cinnamyl alcohol dehydrogenase (CAD) activity converting coniferaldehyde to coniferyl alcohol in *PtrCAD1* RNAi transgenics.

Table S4 Regression analysis of each enzyme activity with cinnamyl alcohol dehydrogenase (CAD) activity converting coniferaldehyde to coniferyl alcohol in *PtrCAD1* RNAi transgenics.

Table S5 Correlation analysis of each enzyme activity with cinnamyl alcohol dehydrogenase (CAD) activity converting sinapaldehyde to sinapyl alcohol in *PtrCAD1* RNAi transgenics.

© 2018 The Authors
New Phytologist © 2018 New Phytologist Trust

14698137, 2019, 1, Downloaded from https://nph.onlinelibrary.wiley.com/doi/10.1111/nph.15505 by CochraneChina, Wiley Online Library on [31/01/2024]. See the Terms and Conditions (https://onlinelibrary.wiley.com/terms-and-conditions) on Wiley Online Library for rules of use; OA articles are governed by the applicable Creative Commons License

Table S6 Regression analysis of each enzyme activity with cinnamyl alcohol dehydrogenase (CAD) activity converting sinapaldehyde to sinapyl alcohol in *PtrCAD1* RNAi transgenics.

Table S7 Enzyme assays of stem-differentiating xylem (SDX) proteins in *PtrCCR2* RNAi transgenics.

Table S8 Correlation analysis of each enzyme activity with cinnamoyl-CoA reductase (CCR) activity converting feruloyl-CoA to coniferaldehyde in *PtrCCR2* RNAi transgenics.

Table S9 Regression analysis of each enzyme activity with cinnamoyl-CoA reductase (CCR) activity converting feruloyl-CoA to coniferaldehyde in *PtrCCR2* RNAi transgenics.

Please note: Wiley Blackwell are not responsible for the content or functionality of any Supporting Information supplied by the authors. Any queries (other than missing material) should be directed to the *New Phytologist* Central Office.

About *New Phytologist*

- *New Phytologist* is an electronic (online-only) journal owned by the New Phytologist Trust, a **not-for-profit organization** dedicated to the promotion of plant science, facilitating projects from symposia to free access for our Tansley reviews and Tansley insights.
- Regular papers, Letters, Research reviews, Rapid reports and both Modelling/Theory and Methods papers are encouraged. We are committed to rapid processing, from online submission through to publication 'as ready' via *Early View* – our average time to decision is <26 days. There are **no page or colour charges** and a PDF version will be provided for each article.
- The journal is available online at Wiley Online Library. Visit **www.newphytologist.com** to search the articles and register for table of contents email alerts.
- If you have any questions, do get in touch with Central Office (np-centraloffice@lancaster.ac.uk) or, if it is more convenient, our USA Office (np-usaoffice@lancaster.ac.uk)
- For submission instructions, subscription and all the latest information visit **www.newphytologist.com**

© 2018 The Authors
New Phytologist © 2018 New Phytologist Trust

14698137, 2019, 1, Downloaded from https://nph.onlinelibrary.wiley.com/doi/10.1111/nph.15505 by CochraneChina, Wiley Online Library on [31/01/2024]. See the Terms and Conditions (https://onlinelibrary.wiley.com/terms-and-conditions) on Wiley Online Library for rules of use; OA articles are governed by the applicable Creative Commons License